EFFECTS OF EXTRUSION PARAMETERS ON THE MECHANICAL PROPERTIES OF ALUMINUM

by

İsmail KARAHAN

B.S. in M.E., Technical University of İstanbul,1982

Submitted to the Institute for Graduate Studies in Science and Engineering in partial fulfillment of the requirements for the degree of

Master of Science

in

Mechanical Engineering

Boğaziçi University

1986

EFFECTS OF EXTRUSION PARAMETERS ON THE MECHANICAL PROPERTIES OF ALUMINUM

APPROVED BY

Doç.Dr.Sabri ALTINTAŞ S. Altıntaş

(Thesis Supervisor)

Doç.Dr.Öktem VARDAR

Y.Doç.Dr.Turan ÖZTURAN

DATE OF APPROVAL :

ACKNOWLEDGEMENTS

I would like to express my most sincere appreciation to my thesis supervisor Doç.Dr.Sabri Altıntaş for his most helpful advice and guidance throughout the course of this work.

I also wish express my gratitude to Prof.Dr.Şefik Güleç, Head of the Material Research Department, for permission to carry out this research in TÜBİTAK.

My grateful appreciation goes to Dr. Mustafa Gevrek for his guidance in theoretical work, to Mr. Suat Tuncel for photography and to Mr.Sinan Onurlu for useful discussions.

I am particularly grateful to Mr.Saadettin Ozan, Mr.Ömer Şafak and Mr. Sadullah Otuk for their careful work in specimen preparation and assistance in performing the tests.

July, 1986 İSMAİL KARAHAN

EFFECTS OF EXTRUSION PARAMETERS ON THE MECHANICAL PROPERTIES OF ALUMINUM

ABSTRACT

The effects of some extrusion parameters, extrusion ratio and initial billet temperature, on the structure and mechanical properties of aluminum are examined.

Initial billet temperature and extrusion ratio determine the structural changes occuring during and after the extrusion process and their contribution to the structure of the product. It is noted that mechanical properties of product also change with these parameters via the structure.

Extrusion ratio effects are recognized in the strain rate which is, then combined with temperature effects in a temperature corrected strain rate term, Z. It is shown that structure and mechanical properties of product are related to, and can be controlled by, Z. Relations between the logarithm of Z and mechanical properties of product are used to develope the extrusion limit diagram so that it shows the mechanical properties of extruded product.

ÖZET

Ekstrüzyon oranı ve ilk takoz sıcaklığı gibi bazı ekstrüzyon değişkenlerinin alüminyumun mikroyapısı ve mekanik özelliklerine etkisi incelenir.

İlk takoz sıcaklığı ve ekstrüzyon oranı, işlem sırasında ve sonrasında olan mikroyapı değişikliklerini ve onların ürün üzerindeki birleşik etkilerini belirler. Ürünün mekanik özelliklerinin de mikroyapıdaki bu değişikliğe bağlı olarak bu işlem değişkenlerinden etkilendiği belirtilir.

Ekstrüzyon oranı etkisi, şekil değiştirme hızı olarak gözönüne alınıp, sıcaklık etkileri ile sıcaklık dengelemeli genleme hızı, Z, teriminde birleştirilir. Ürünün mikroyapısının ve mekanik özelliklerinin Z ile ilgili olduğu ve bu değişkenle kontrol edilebileceği gösterilir. Log Z ile ürünün mekanik özellikleri arasındaki bağlantılar ekstrüzyon sınır diyagramının ürünün mekanik özelliklerini gösterecek şekilde geliştirilmesinde kullanılır.

TABLE OF CONTENTS

LIST OF FIGURES

Page

LIST OF TABLES

LIST OF SYMBOLS

A_1, A_2, A_3 : Material constants

B_1, B_2, B_3 : Material constants

d : Mean subgrain diameter

D_B : Billet diameter

D_E : Die diameter

h : Depth of recrystallized layer

ΔH : Activation energy for hot working

K : Subboundary strengthening coefficient

$K_1 \ldots K_7$: Constants in heat equation

L : Billet length

n : Strain hardening exponent

p : Extrusion load

P_{max} : Maximum extrusion load

r : Distance from the centerline of the product

R : Extrusion ratio

t : Time, extrusion time

T : Deformation temperature

ΔT : Temperature rise during extrusion

T_o : Initial billet temperature

V : Extrusion speed

W	: Semiangle of deformation cone
Z	: Temperature corrected strain rate
Z_i	: Initial temperature corrected strain rate
$Q_1 \ldots\ldots Q_7$	: Heat flows
ε	: Strain rate
α	: Material constant
σ	: Flow stress
σ_i	: Internal stress
σ^*	: Effective stress
σ_y	: Yield stress
$\sigma_{0.2}$	: Proof stress
σ_{UTS}	: Ultimate tensile strength

I. INTRODUCTION

Deformation is one of the several processes which may be used to obtain intermediate or final shapes in metals. The applicability and development of these types of processes are completely dependent on the plasticity of the solid metal. The study of plasticity is concerned with the relationships between metal flow and applied stress. If these can be determined, then the required shapes can be achieved by the application of calculated forces, in specified directions, at controlled rates. In practice, the external load is applied by a tool and its shape controls the direction of application necessary to achieve the desired flow. The type of tool can be used to classify the different categories of deformation processes. Common industrial processes fall into six categories; deep drawing, rolling, forging, stretching, extrusion, wiredrawing. Although there are other processes, e.g. roll forging, spray forming, etc., these are not of any great industrial significance [1].

In extrusion process, besides the fact that prediction of the metal flow and temperature changes during extrusion is hard to handle, the problem of choosing suitable die

materials to withstand the high temperatures and pressures required to extrude the harder, stronger materials are not overcome. Nowadays, it is possible to extrude successfully the following metals and their alloys; aluminum, copper and lead [1]. Although a special technique is required, the extrusion of steel is also possible.

There are two kinds of extrusion; direct and indirect. In the former case, the ram and die are at opposite ends of the billet and the metal is pushed up to and through the die as represented in Fig.1.

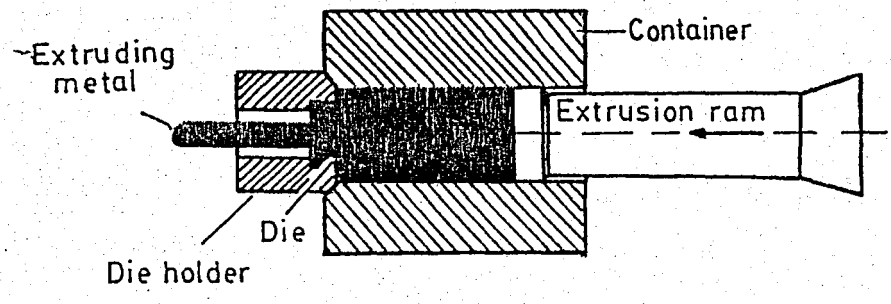

FIGURE 1. Direct extrusion process [1].

With direct or inverted extrusion, the die is held at the end of the hollow ram and is forced into the billet so that metal is extruded backwards through the die as represented in Fig.2.

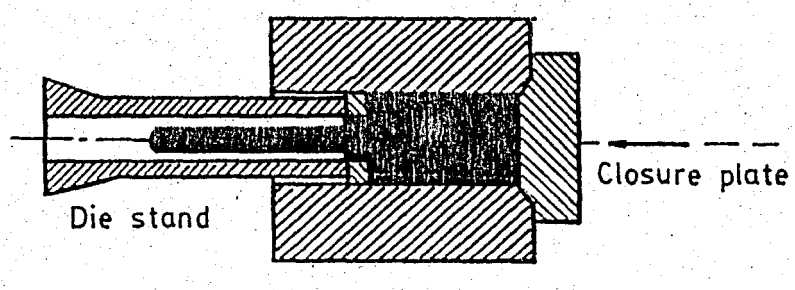

FIGURE 2. Indirect extrusion process [1].

II. EXTRUSION OF ALUMINUM

A. EXTRUSION PROCESS PARAMETERS

Attempting to describe the relations between extrusion parameters is difficult, since this process has many parameters and interactions between these parameters are complex. Fig.3 shows these interactions in direct extrusion. It has been reported that initial billet temperature, extrusion ratio and speed are directly effective parameters on the microstructure of the product [2-3] . Initial billet temperature determines the temperature of deformation and, extrusion ratio and extrusion speed determine the strain rate during this process.

The strain rate varies from point to point throughout the deformation zone during the extrusion process so, it is necessary to define some average value for this parameter. There are two techniques, which appear to be acceptable, to calculate average strain rate : finite-elemant technique and the minimized upper-bound solution. Most previous researchers have used the approach suggested by Feltham [2]. According to Feltham, the mean strain rate may be written as.

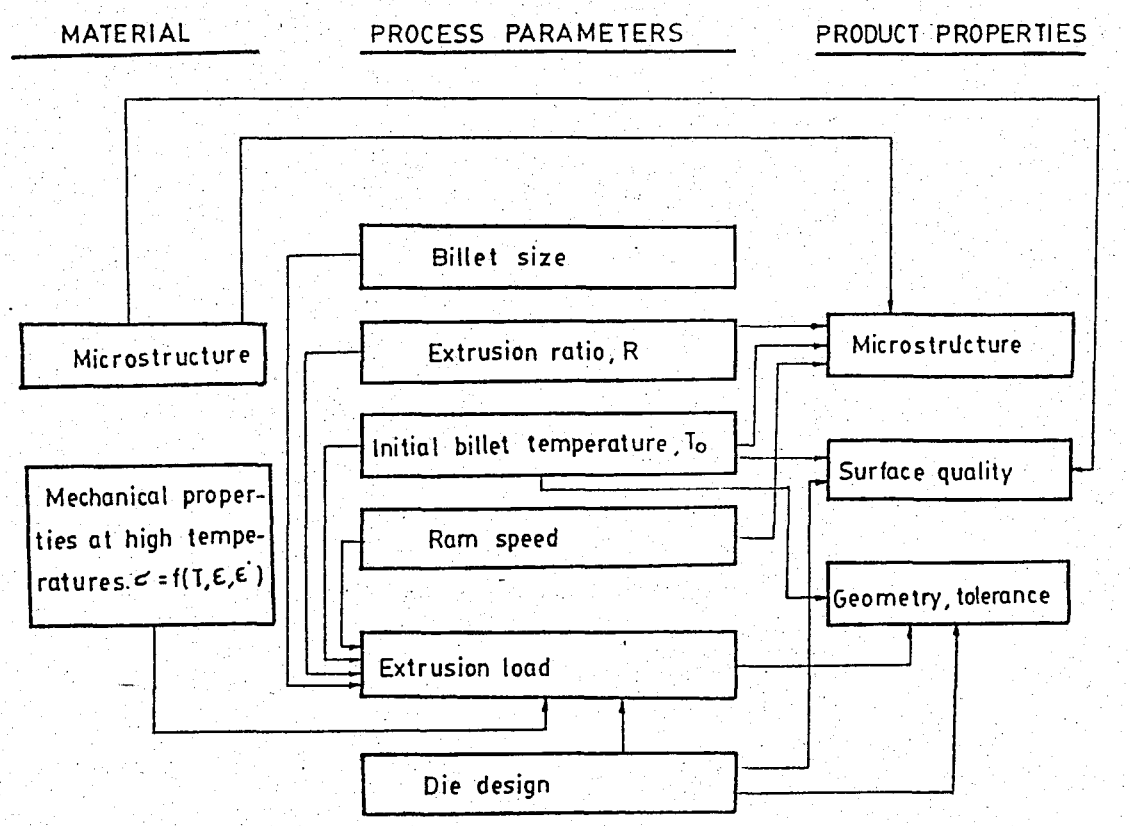

FIGURE 3. Interactions between the properties of material and product and process parameters in the direct extrusion. [3]

$$\dot{\varepsilon} = \frac{\text{total strain}}{\text{time taken to effect that strain}} \qquad (1)$$

Total strain is given by a constant, c, and the time taken to effect this strain can be easily calculated as [2]

$$\frac{D_B^3 - D_E^3}{6.D_B^2.v.\tan w}$$

giving

$$\dot{\varepsilon} = \frac{6.\bar{c}.v.D_B^2.\tan w}{D_B^3 - D_E^3} \qquad (2)$$

where D_B = Billet diameter,

D_E = Die diameter,

v = Extrusion speed,

w = Semiangle of deformation cone.

Sheppard [2] has given the relations (determined by using upper-bound solution and verified by inspection of macro-etched billet) :

$$w = 54.1 + 3.45\ \text{LnR} \qquad (3)$$

$$c = \text{LnR} \qquad (4)$$

for 1100 alloy. R is extrusion ratio.

During the extrusion processes, energy dissipated is converted to thermal energy resulting in temperature variations

both traverse to and perpendicular to the ram travel. Traverse variations in temperature produce variations in structure,and hence in properties, across the extruded section. However, since it is the bulk properties which are important and, in any case, structural differences across the section are difficult to determine, it is acceptable to calculate an average temperature rise at any instant [3].

Factors affecting the temperature rise may be quantified by placing a control volume around deformation zone and equating the heat leaving this volume to the work put into it [3]. Since the billet is also losing heat to container, outside this area, a second control volume may be used to include this heat loss in overall equation. The heat losses are shown in Fig.4. Assuming that 90% of the work is converted into heat, the following applies

$$0.9\ P.v.t = Q_1 + Q_2 + Q_3 + Q_4 + Q_5 + Q_6 + Q_7 \qquad (5)$$

where P = Extrusion load,

v = Ram speed,

t = Extrusion time,

Q_1 = Heat loss from deformation zone to dead zone,

Q_2 = Heat loss from deformation zone to container,

Q_3 = Heat loss from product to die,

Q_4 = Heat loss from deformation zone to billet,

Q_5 = Heat loss from billet to container,

Q_6 = Heat loss from billet to ram,

Q_7 = Heat loss from deformation zone to product.

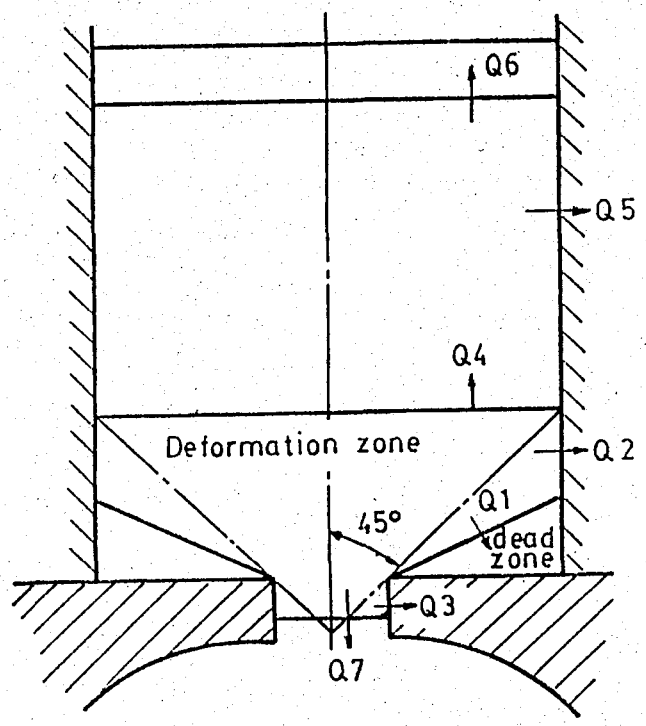

FIGURE 4. Heat flows during the extrusion process [3].

Sheppard [2] has calculated the heat losses and solving the heat equation, he has given the equation for temperature rise as

$$\Delta T = \frac{0.9\ P.v.t - \Delta T_p.\ C_2(t)}{C_1(t)} \qquad (6)$$

$$C_1(t) = K_1\ t^{1/2} + K_2\ t^{2/3} + K_3\ t$$

$$C_2(t) = K_4\ t^{1/2} + K_5\ t^{3/2} + K_6\ t^{4/3} + K_7\ t^{5/3}$$

where ΔT = Temperature rise,

ΔT_p = Temperature differential between product and tool,

K_{1-7} = Constants related to heat losses [2].

More recently, M.Gevrek [4] have developed a finite-difference algorithm to calculate temperature distribution

on the deformation zone during extrusion. This programme was used in this study to calculate the temperature rise during extrusion. Fig.5 shows the temperature increase of the product calculated by this programme as a function of product length at a given extrusion ratio, R=25 and initial billet temperature, T_o = 350 ^oC. Detailed information about this programme is given in Appendix A.

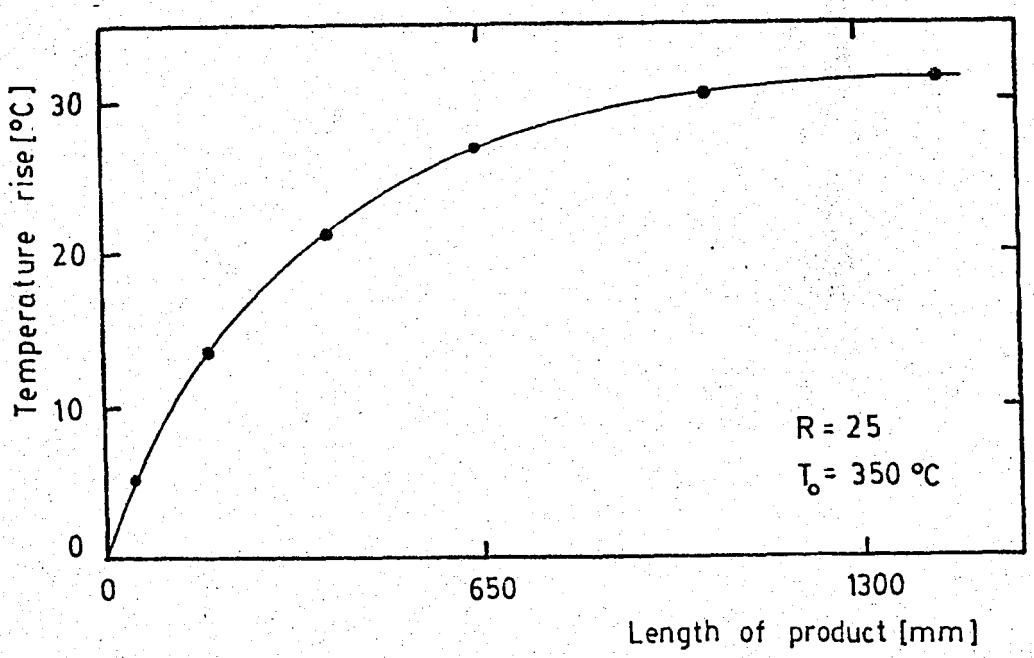

FIGURE 5.A typical temperature rise curve during extrusion .

Average strain rate values for the specimens were also calculated by means of a computer programme which gives the strain rate values for 30 points throughout the diameter of the product [4]. Variation of the strain rate with the distance from the centerline of the rod is given in Fig.6. Strain rate at the center of the product is higher than the one at the surface. An average of the strain rate values corresponding to the points inside the specimen diameter was taken into account.

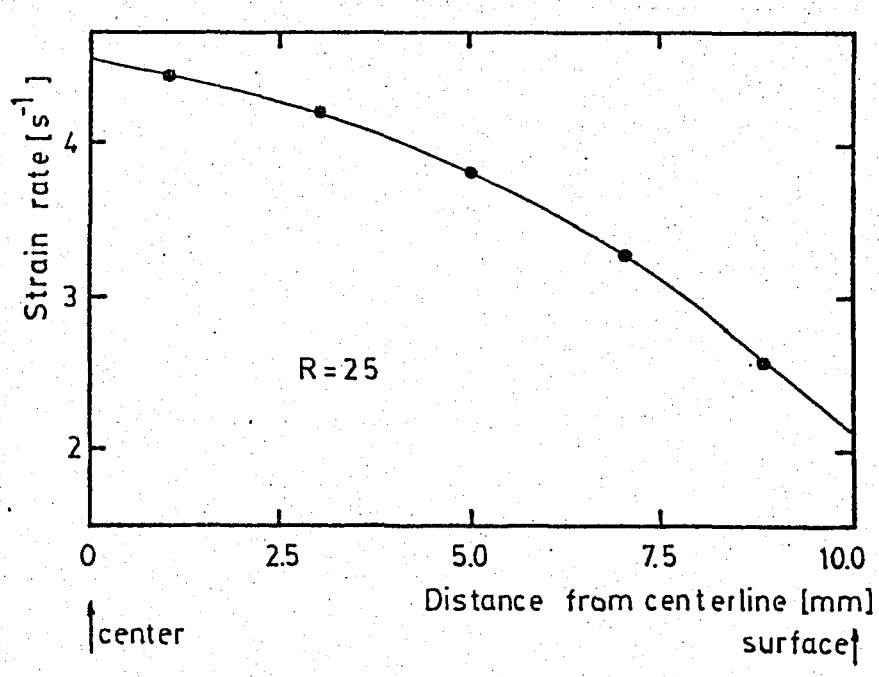

FIGURE 6. Variation of strain rate with the distance from the centerline of the rod.

Detailed information about this computer programme is given in Appendix B.

B. STRUCTURAL CHANGES OCCURING DURING AND AFTER EXTRUSION

Almost all metals, excluding some castings, are hot-worked during processing into a final product. Most of these hot-worked materials go into service in the as-deformed state in the form of products such as steel plate or aluminum extrusions. Whether as an intermediate or as a final product, the properties of such hot-deformed materials are determined by the working process. Therefore, one should consider the structural changes occuring both during and after working, and describe the influence of these changes on the mechanical

properties of the worked material.

The restoration mechanisms in hot working can be divided into dynamic ones in the deformation zone and static ones in the cooling zone (Fig.7). Metals of high stacking fault energy like aluminum undergo dynamic recovery at both low and high

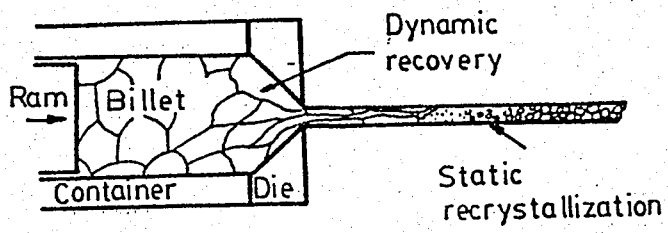

FIGURE 7. Softening mechanisms effective during and after extrusion of Aluminum [5].

strains followed by static recovery and recrystallization respectively. Metals of low SFE like copper undergo dynamic recovery and,in addition, dynamic recrystallization at high strains, followed in both cases by static recrystallization [5].

Aluminum is a metal of high SFE. It undergoes dynamic recovery during the extrusion process. This is followed by static recovery and static recrystallization after extrusion [6-8]. In Fig.8 substructures of aluminum are given for undeformed, deformed to 0.1, steady state at 0.5 and steady state at 2.0 conditions. Dynamic recovery, static recovery and static recrystallization will be discussed in details below.

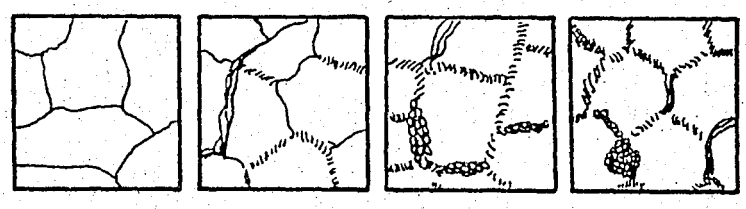

FIGURE 8. Substructure development in Aluminum during the hot working [5].

a) Dynamic recovery

When a recrystallized metal is loaded at constant nominal strain rate, the resulting flow curve can be divided into three distinct stages The first stage is that of micro-strain deformation occuring as the plastic strain rate in the sample increases from zero to the approximate strain rate of the test [3]. (Fig.9) During this interval the state of stress in the material rises rapidly although not quite as steeply as it does at conventional temperatures. Typical loading slopes during initial loading range are around E/50 at high temperatures and high strain rates. The loading slopes are not comparable with the modulus because of the plastic strain produced during the loading interval prior to the microscopic flow. This strain arises from the operation of the thermally activated mechanisms that are rate controlling in this temperature range and, therefore, increases with increasing temperature and decreasing rate of loading.

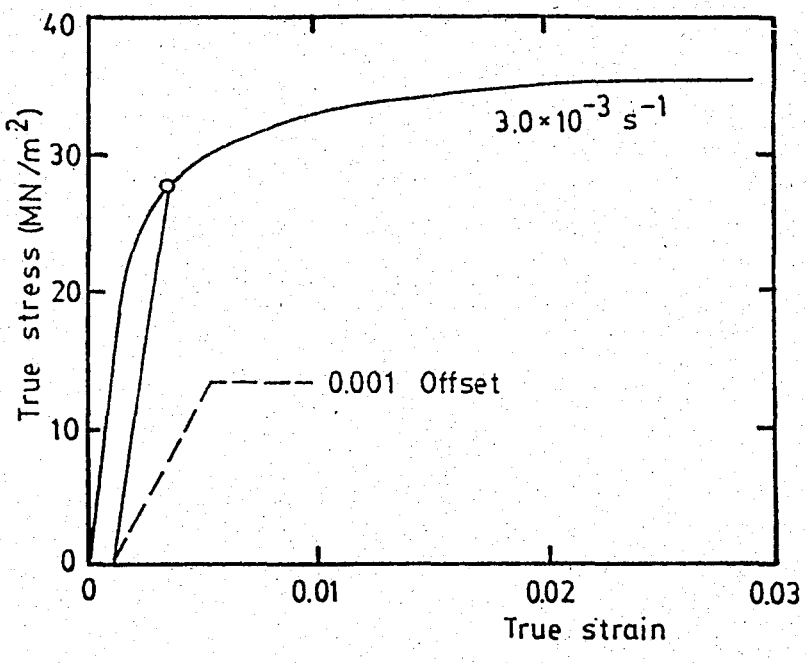

FIGURE 9. Flow curve of aluminum at high temperatures.

The end of the microstrain interval is signified by a decrease in the slope of the loading curve about an order of magnitude. Yield drops are not, in general, observed and the yield stress is defined instead in the term of a plastic strain offset of 0.1 or 0.2 %. (Fig.9) The region of the yield stress marks the beginning of the work hardening and, the slopes are again temperature and rate sensitive. During this second stage deformation, the work hardening rate gradually decreases until the net rate of work hardening is zero. This regime, named steady state regime, is characterized by constancy of three parameters: stress, temperature and strain rate. It should be considered that the microstructural changes accompany the three stages of flow curve depicted in Fig.9. Some dislocation multiplication takes place during the microstrain interval and

the dislocation density increases. It continues to increase with strain after yielding at a slower rate and attains a constant value in steady state region [9]. During the phase of positive strain hardening, the dislocations begin to form a cellular structure. By the time the steady state regime is attained, the dislocation have arranged themselves into subgrains whose perfection, dimensions and misorientations depend on the metal and on the strain rate and temperature of deformation [10]. This condition of essentially constant dislocation density, which is necessary for the absence of strain hardening results from the attainment of the dynamic equilibrium between dislocation generation and annihilation. The stable subgrain size depends on the equilibrium dislocatic density which is established by this balance.

The higher the temperature of deformation and the lower the strain rate, the larger are subgrains that are formed during high temperature deformation. As they increase in size, the subgrains contain fewer dislocations. This structural variation reflects the diminution in the equilibrium dislocat density arising from the increase in temperature and decrease in strain rate. The generation rate decreases, because effect stress decreases with decreasing strain rate and with increas temperature. The annihilation rate, on the other hand, does not decrease as much with a decrease in strain rate, because it is not sensitive to a stress decrease as the generation rate is.

The dependence of mean subgrain diameter, d, on the temperature, T and strain rate, $\dot{\varepsilon}$ is described by the relation:

$$d^{-m} = a + b \text{ Ln } Z \tag{7}$$

where a and b are empirical constants m is a material constant and Z is the temperature corrected strain rate which is defined by the relation :

$$Z = \dot{\varepsilon} . \exp (\Delta H/GT) \tag{8}$$

where ΔH = activation energy for hot working,

and G = Universal gas constant.

At high temperatures, it is common to express the flow stress, σ, as

$$\sigma = \sigma^{*} + \sigma_i \tag{9}$$

where σ^{*}, known as the effective stress, is the reversible component of the flow stress, changes in which are concurrent with changes in temperature or strain rate. The term σ_i refers to the irreversible or structural component of flow stress, also known as the internal stress. If σ^{*} remains approximately constant with strain and setting [9]

$$\sigma_i = K d^{-1} \tag{10}$$

where K is the subboundary strengthening coefficient, we can

write that::

$$\sigma = \sigma^{*} + Kd^{-1} \qquad (11)$$

Yield stress, σ_y is an approximately constant fraction of flow stress in most material. Thus, if the only softening mechanism is dynamic recovery, one can write by combining the Eq.7 and Eq.11

$$\sigma_y = A + B\ LnZ \qquad (12)$$

Here, A and B are empirical constants.

b) Static recovery and static recrystallization

Static softening processes take place after deformation is complete or between intervals of hot-working. These processes can be divided into two distinct categories :

i) The recovery process which involves the annihilation of dislocations in individual events.

ii) The recrystallization process, in which dislocations are simultaneously eliminated in large numbers as a result of the motion of high angle boundaries.

The main experimental variable affecting the recovery rate are the temperature, strain and strain rate[11].The effect of temperature is evident but is not particularly marked, because the amount of stored energy driving the recovery decreases as the deformation temperature is increased. It is

also apparent that the rate of recovery decreases with time indicating that the stored energy or driving force is progressively reduced by the operation of the recovery process [11]. Because the driving force for recovery is generally different at different deformation temperatures, it is difficult to determine the activation energy associated with static recovery, after high temperature deformation. In general, increases in strain lead to increase in the recovery rate, until steady state flow is achieved. This can be attributed to the increase in dislocation density, and therefore driving force, with strain until equilibrium is reached.

Static recrystallization has been reported frequently in literature [12-15]. The time for complete recrystallization increases with the deformation temperature. The recrystallized grain size also increases with temperature, confirming the strong influence of subgrain size and driving force on the processes of the nucleation and growth. Increasing the strain rate of deformation decreases the incubation time and increases the rate of subsequent recrystallization. Finer grains are produced by deformation at higher strain rates because of the reduced grain sizes formed by dynamic recovery at lower values of temperature corrected strain rate. The increase in recrystallization rate with strain is accompanied by a decrease in recrystallized grain size.

2. Structure of the aluminum products

a) Microstructure

The considerations above indicate that microstructures of the aluminum alloys after extrusion are likely to be complex

because of the heterogeneous nature of the deformation. Although dynamic recovery is usually the mechanism operative during deformation, the strain, strain rate and temperature conditions at the periphery of product may be suitable to provide the driving force necessary for static recrystallizatio to occur at this location [8].

Most of the researchers reported using materials which dynamically recover, have been related to the extrusion of aluminum and its alloys [16-22]. These researchers observed that, the microstructure most usually appears "fibrous". The structure consists of the original cast grains elongated into the extrusion direction and having a ratio roughly equal to the extrusion ratio. The fibrous effect is due to the high angles existing between the string-like grains. Although static recovery may occur after the extrusion, static recrystallizatio does not.

Incorrect extrusion conditions may lead to gross heterogeniety in the product in which the surface layer recrystallizes to produce large recrystallized grains. This is least desirable structure. Sheppard [6] has given a linear relationship

$$h = M + N \, \mathrm{Ln}Z \qquad (13)$$

where M and N are empirical constants and h is the recrystallization depth. Stress corrosion susceptibility and heat treatment sensitivity indicate the need to predict when extrusion will produce a recrystallized structure. The method

most commonly used is to plot hardness values v.s. extrusion temperature. But in extrusion, some other parameters such as strain rate and cooling conditions, are also effective. Raybould and Sheppard [2] have reported that the Al-7% Zn alloy had a minimum LnZ value of 28.55 to recrystallize when it was water-quenched. In general, this may be written as

$$T_R = \frac{H}{G.Ln(Z_R/\dot{\varepsilon})} \qquad (14)$$

where Z_R is the critical temperature corrected strain rate value for recrystallization.

b) Substructure

It has been suggested that it is the effective stress upon a dislocation and the distance moved which uniquely determines deformation characteristics in such a way that Z should relate the final properties of a metal under differing deformation conditions. The final properties are most conveniently represented by the subgrain diameter and will depend upon the quench rate. In literature [6,8,19,23], for air cooled products and for different material, some parametric equations have been given as;

$$d^{-1} = 0.15\ LnZ\ -3.5 \qquad \text{(AA 2014)} \qquad (15)$$

$$d^{-1} = 0.044\ LnZ\ -0.884 \qquad \text{(Commercially pure AL)} \qquad (16)$$

$$d^{-1} = 0.037\ LnZ\ -0.67 \qquad \text{(AL-Li-Mg)} \qquad (17)$$

$$d^{-1} = 0.0058\ LnZ-0.1733 \qquad \text{(AA 1100)} \qquad (18)$$

c) Effect of precipitation

It has been shown that both precipitations during extrusion and the quenching type after extrusion may have some effects on the mechanical properties of product [7,18,24] and the extrusion parameters, hence quenching type should be chosen according to age hardening features of the material [25].Paterson and Sheppard [7] have observed that AA 2014 alloy has softened considerably, despite the structural differences observed has been constant for all of the extrudates.(Fig.10)

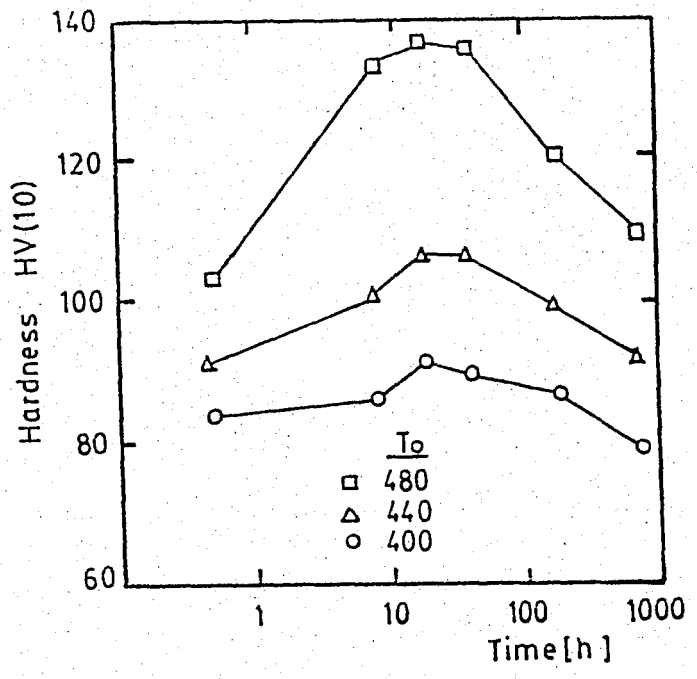

FIGURE 10. Hardness variation with the aging time [7].

The retained substructures do not seem to contribute to strength for some alloys. The strength of the alloy can be improved by natural aging at room temperatures or by artificial aging at elevated temperatures. The greater, the amount

of solute in solution, the greater the influence of the zones which act as obstacles to dislocation motion and make material more strong. Despite that there is a little amount of solute in commercial pure aluminum, it has been observed that whether fine or coarse dispersion of precipitation may have a considerably important effect on the mechanical properties of this material [21].

C. EXTRUSION LIMIT DIAGRAM

1. Restrictions on working conditions

The choice of the temperature range for hot working is important. During the deformation process, the heat of the deformation may cause a temperature rise, if the strain rate is so high that conditions are approaching adiabatic. On the other hand, if the strain rate is low, heat may be lost to the surrounding and the temperature of the workpiece will drop as it is deformed. The finishing temperature will have a marked effect on the structure and the properties of product. If the temperature is high, then the final grain size will be coarse, affecting the mechanical properties. If, on the other hand, deformation rates cause adiabatic conditions, the resulting temperature rise of the metal might exceed the solidus, giving rise to incipient melting.

Smith [26] has shown that the extrusion temperature and the strain rate must be jointly controlled, if the defects are to be avoided. The working range of an alloy can be illustrated in a diagrammatic manner by considering the metal

temperature and the amount of deformation. The effect of strain rate can be added later to the diagramme so that all the variables controlling working range are included. For a given working pressure and temperature, there will be a maximum amount of deformation that can be carried out on the metal. If the working pressure is maintained, the amount of deformation possible will increase, if the temperature of the metal is increased due to the fact that flow stress is lowered. In Fig.11, this is illustrated by line AB which seperates those areas in which deformation is possible from those in which it is not, for a given applied pressure. The area in which deformation is possible, is restricted at higher

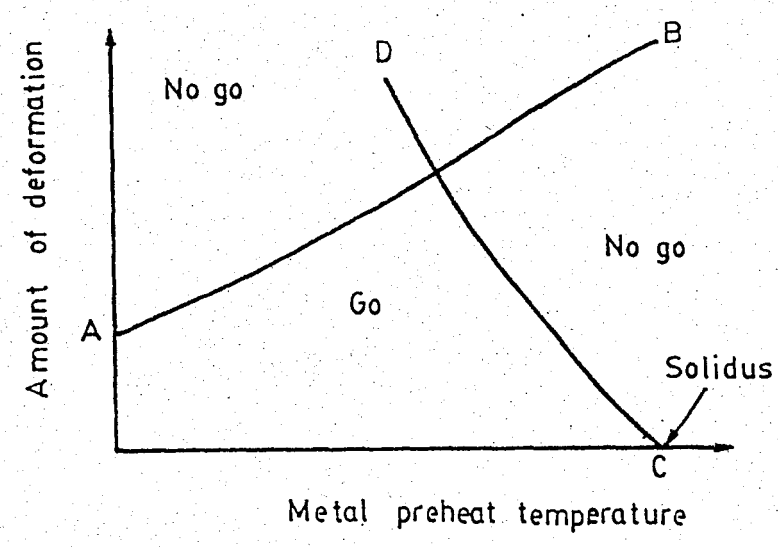

FIGURE 11. Working range for a deformation process [1].

temperatures due to the risk of incipient melting. If deformation is carried out very slowly, the limiting temperature is solidus. If, however, deformation is carried out at faster rates and some energy of deformation appears

as a temperature rise, then the temperature of the metal must be restricted. The greater amount of deformation, the greater the temperature rise. Therefore, a line CD which has a negative slope will limit the upper temperature of working range. The effect of the other possible variables, pressure and strain rate can be included to the diagram as shown in Fig.12. Increasing the applied pressure will increase the

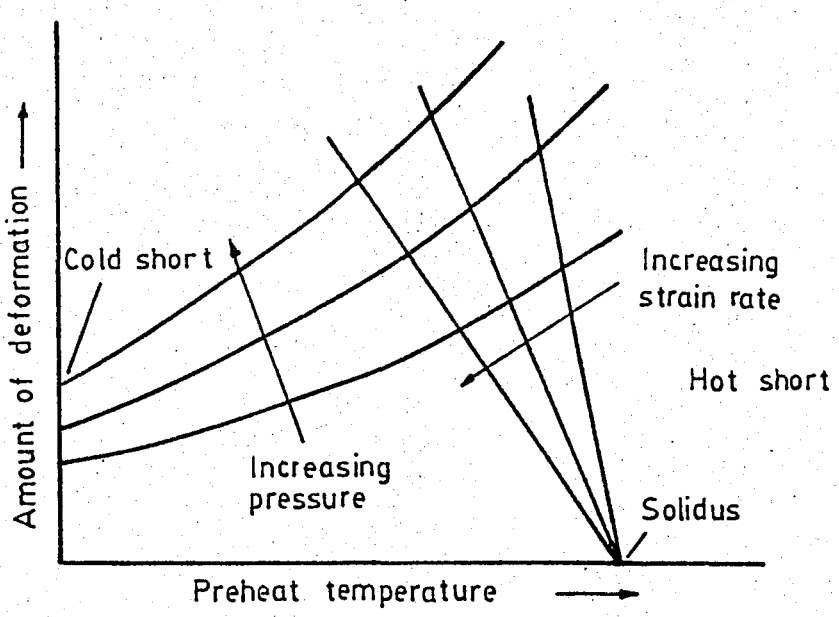

FIGURE 12. Variation of working range with strain rate and pressure [1].

deformation range whilst increasing the strain rate will have the opposite effect.

Extrusion process is limited by the capacity of the press and melting of the material extruded. The extrusion load, which depends on the flow stress of the material at elevated temperatures should not exceed the press capacity. Incipient

melting restricts the initial billet temperature. These two limitations can be shown in a diagram, called "extrusion limit diagram". Fig.13 shows a simple limit diagram in which temperature are plotted against the logarithm of extrusion ratio to be used for choosing of possible working conditions

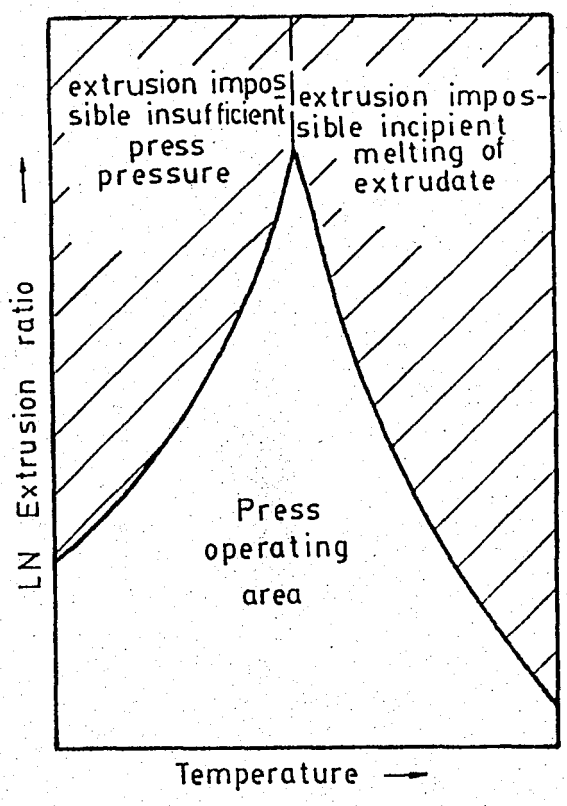

FIGURE 13. Simple extrusion Limit diagram [7].

in which press capacity and material properties are determined for a constant velocity.

To draw the pressure limit, a formulation, which determine the extrusion pressure as a function of the flow stress and the extrusion process parameters, should be derived.

For constant initial billet temperature, T_o, extrusion speed, v and billet length, L, maximum extrusion pressure

increases linearly with the logarithm of extrusion ratio, R [3] :

$$P_{max} = (A_1 + B_1 \, LnR)_{T_o,v,L} \qquad (15)$$

where A_1 and B_1 are constants depending on the extruded material and extrusion conditions.

For constant extrusion speed, extrusion ratio and billet length, maximum extrusion pressure decreases linearly with the initial billet temperature [3] :

$$P_{max} = (A_2 - B_2 \, T_o)_{R,v,L} \qquad (16)$$

where A_2 and B_2 are constants depending on the extruded material and extrusion conditions.

Considering that material flow stress at high temperature depends on the strain rate, maximum extrusion pressure will be clearly dependent on both temperature and strain rate [3]. These parameters are combined in the temperature corrected strain rate, Z. Then, for constant billet length and extrusion ratio, we may write

$$P_{max} = (A_3 + B_3 \, LnZ)_{R,L} \qquad (17)$$

where A_3 and B_3 are material constants. Thus, extrusion pressure can be determined as a function of extrusion and material parameters, by combining Eqs. 15,16 and 17, for constant temperature :

$$P_{max} = \sigma(A + B\ LnR) \tag{18}$$

For high stresses, it has been shown that flow stress of material at elevated temperatures depends on the strain rate and temperature by the equation [6,27]:

$$\sigma = \frac{1}{\alpha . n} \left(Ln \left(\frac{Z}{A^*}\right) - \frac{\Delta H}{GT} \right) \tag{19}$$

where α and n are material constants. Substituting Eq.19 into Eq.18 :

$$P_{max} = \frac{1}{\alpha . n} \cdot \left(Ln\left(\frac{Z}{A^*}\right) - \frac{\Delta H}{GT}\right) . (A+B\ LnR) \tag{20}$$

or in general form

$$P_{max} = \frac{1}{\alpha . n} \left(a + b\ LnR + c\ Ln \frac{Z}{A^*}\right) \tag{21}$$

may be written. a, b and c can be determined by the experiments which are performed for constant billet length. Thus, constant pressure limit on extrusion limit diagram can be plotted by using Eq.21.

In literature, to verify the form of Eq.21, the extrusion data has been subjected to multiple regression analysis for some aluminum alloys and reported as given below [3,27] :

$$P_{max} = \frac{1}{\alpha . n} (12,48\ LnR + 5.65\ Ln \frac{Z}{A^*} - 15.692)\ (AA1100) \tag{22}$$

$$P_{max} = \frac{1}{\alpha.n}(13.14\ LnR + 4.3\ Ln\ \frac{Z}{A^*} - 3.33) \quad (AA2014) \quad (23)$$

$$P_{max} = \frac{1}{\alpha.n}(17.3\ LnR + 10.3\ Ln\ \frac{Z}{A^*} + 11.2) \quad \begin{matrix}(Commercial \\ pure\ AL)\end{matrix} \quad (24)$$

The actual working temperatures should be used to determine both the flow stress and incipient melting line. The upper-bound solutions indicate that most of the work done during extrusion occurs at the maximum temperature rather than the initial temperature. It has been shown that the working temperature remains relatively constant during steady-state extrusion. "Integral profile"temperature shows good correlation with experimental results [28]. Having calculated the temperature, it is still not clear what the limiting temperature line should represent. The main criterion in aluminum alloy production is the surface finish of the product, thus indicating that this is parameter which should determine the temperature locus on the limit diagram [27].This phenomenon is a particular problem during the extrusion of high strength aluminum alloys such as 2014. Although the ductility of aluminum alloys generally increases with temperature, the flow stress decreases such that as the temperature of extrusion is increased, tensile fracture can be induced by the tensile stresses imposed by friction conditions It has been shown that the defining line good and unacceptable surfaces could be represented by a relationship [27]. It has been reported that the condition for acceptable surface could be represented by a relationship.It has been reported that the condition for acceptable surface finish for 2014 alloy is [27]

$$\ln Z < 6900 / T^{0.86} \qquad (25)$$

By plotting the parameter Ln(Z/A) against the initial billet temperature, different aluminum alloyscan be compared. A is a material constant. Such a comparison is shown in Fig. 14 for alloys 2014,7075 and 5456. It has been noted that the

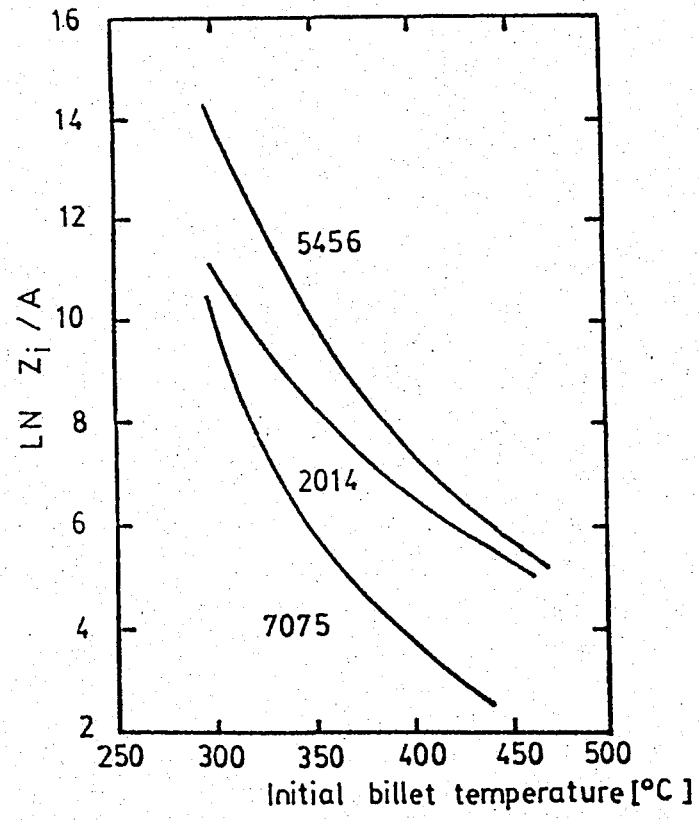

FIGURE 14. Surface cracking boundaries for some aluminum alloys [27].

propensity for surface cracking increases fromthe 5456 to the 2014 and up to the 7075 alloy which is consistent with the corresponding increase in the pressure required for the high temperature extrusion of these alloys [27].

Eq.21 and Eq.25 may be combined within a single graph to show the limiting extrusion conditions. Such a graph is

shown in Fig.15, indicating the possible working conditions for the extrusion speeds of 3.2 and 6.8 mms^{-1} without surface cracking.

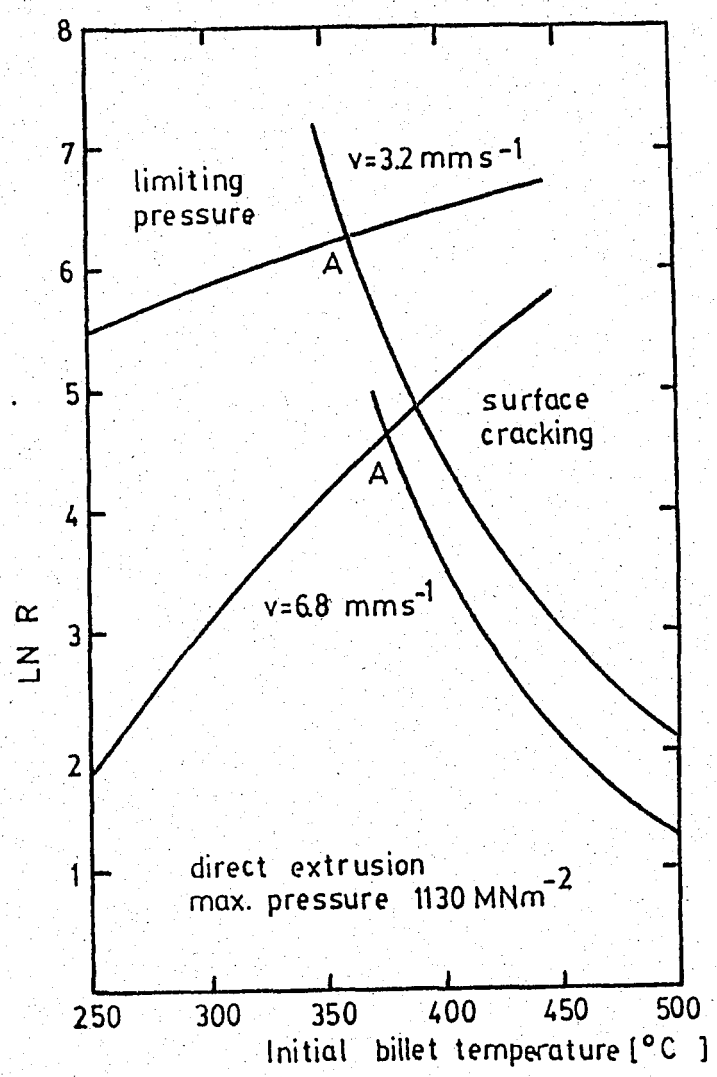

FIGURE 15. Extrusion Limit diagram for 2014 Alloy [27].

2. Structural considerations on limit diagram

Sheppard and Raybould [29] have shown how the extrusion limit diagram may be constructed to give information on the structure of product. It is clear that both desired structure and property parameters may be presented on the extrusion limit diagram.

Fig.16 shows a limit diagram of AL-Cu Alloy indicating subgrain diameter variation with extrusion parameters for a constant ram speed of 10 mms^{-1} [6].

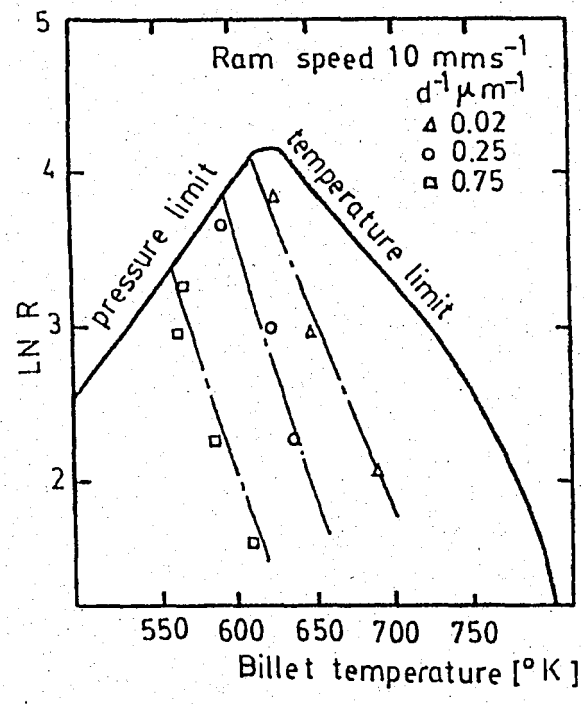

FIGURE 16. Structural limit diagram for AL-Cu alloy [6].

Fig.17 shows the mechanical properties of product for 99.99 % AL. In this diagram, proof stresses, recrystallization boundary and predicted maximum recrystallization temperatures are shown as a function of initial billet temperature and extrusion ratio [29]. In this graph, recrystallization boundary shows the beginning of the recrystallization, predicted maximum recrystallization temperature boundary shows the beginning of the incipient melting and proof stress curves show the extrusion conditions corresponding to the given proof stresses of products.

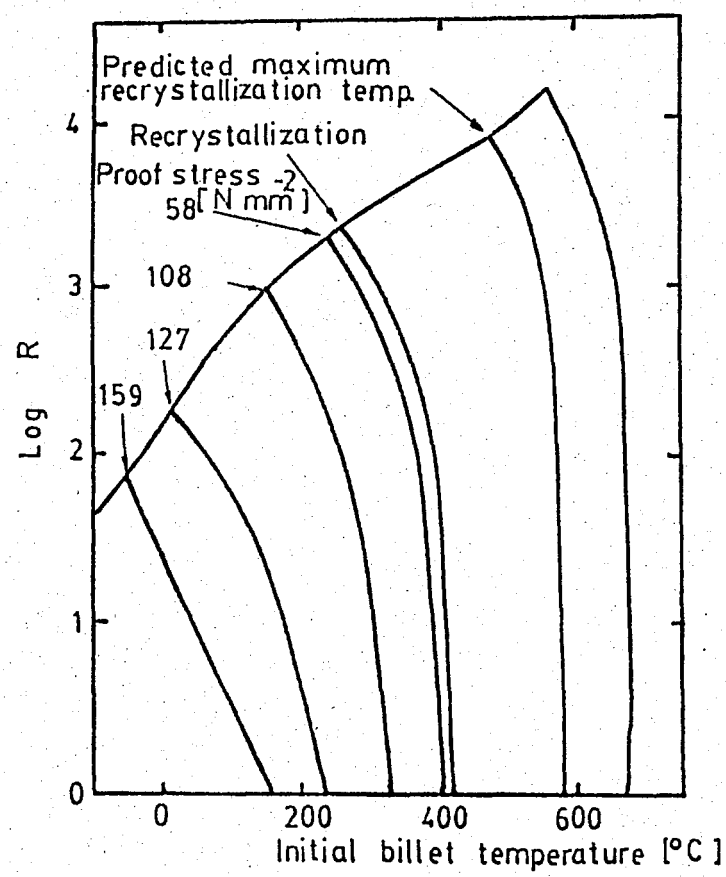

FIGURE 17. Limit diagram showing mechanical properties of the product for 99.99% AL; water-quenched; $\dot{\varepsilon}$ = 16 s^{-1}; maximum pressure = 1100 N/mm^2 [29].

III. EXPERIMENTAL WORK

A-EXPERIMENTAL PROCEDURES

1. Extrusion process

Cylinder billets of commercially pure aluminum, which have 100 mm. in diameter and 100 mm.in length, were extruded at 350, 400 and 450 ^{o}C initial billet temperatures, using a vertical Enefco hydraulic press of 500 ton capacity,(Fig.18) to produce 8,12.5 and 20 mm. rods (Extrusion ratios; 160:1, 63:1, 25:1).

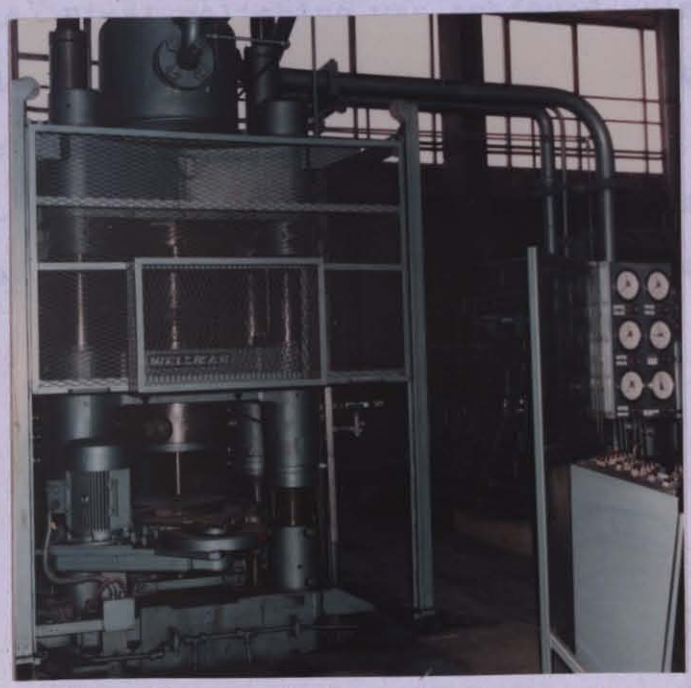

FIGURE 18. Vertical Enefco hydraulic press .

Air cooling was performed. Chemical composition of the material is given Table 1.

TABLE 1. Chemical composition of the extruded material.

Element	Fe	Cu	Mn	Mg	Zn	Si	AL
Weight %	.19-.21	.07-.004	.015-.022	.54-.61	.024-.027	.124-06	Othe

2. Metallographic examinations

Longitudinal and traverse sections were cut from the extrudate and prepared for optical examination. To examine the microstructures of the products at same conditions for different extrusion ratios, all specimens were chosen from the middle sections of the rods. The longitudinal sections were cut from the products and mounted in bakkelite, ground on 200 and 600 grade SiC papers and polished using 6μm diamond paste. Final polishing was achieved using 0.3μm aluminum powder. Using the equipment shown in Fig.19, the specimens were electroetched for three minutes in an acid solution (4mL HBF_4 + 200 mL H_2O) with specimens as anode, with a potential of 12 V applied with a maximum current density of 0.2 A/cm^2 [30].

FIGURE 19. Lectropol electroetching and electropolishing equipment .

The specimens were inspected under polarized light by means of a Reichert optical microscope (Fig.20).

FIGURE 20. Reichert optical microscope .

Recrystallized grain diameters were measured from the photographes using ASTM-E-112 standard, Lineal (Heyn) intercept method for the specimens extruded at 350, 400 and 450°C initial billet temperatures with the extrusion ratios of 25:1 and 160:1.

3. Microhardness measurements

Microhardness measurements were performed on the mechanically polished surfaces with a load of 200 gr. by means of a microhardness test equipment (Fig.21). To eliminate the

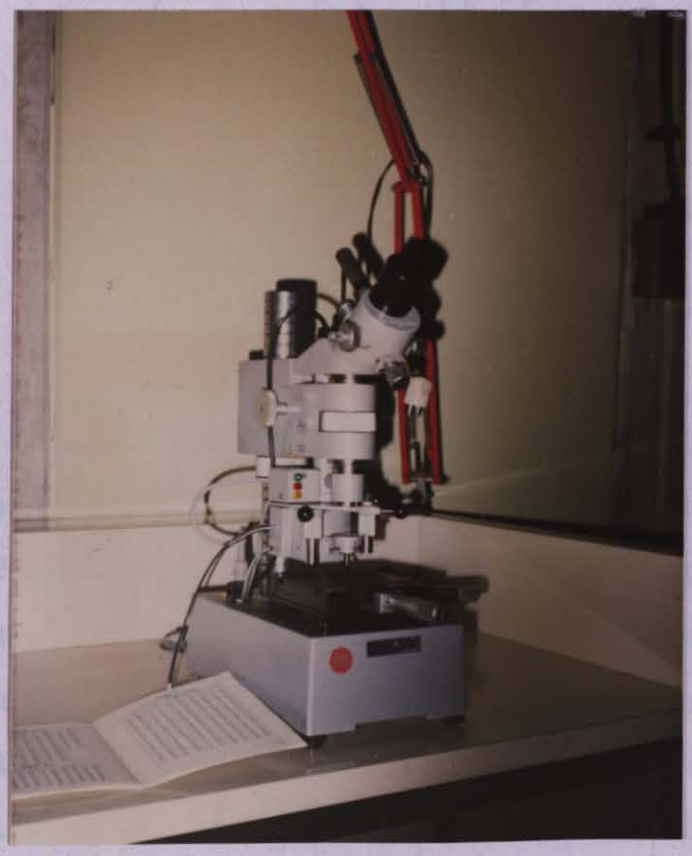

FIGURE 21. Microhardness test equipment.

hardened layer produced by mechanical polishing, electropolishing was performed. Specimens were polished mechanically in the same way described for specimens of metallographic

examination. Then, they were electropolished in an acid solution (40% Percloric acid + ethyl alcohol) with a potential of 20 v/cm^2. As a result of this process, a layer of about 250μm was eliminated. Average of 6-10 readings through the diameter determined the microhardness values of specimens (Fig.22).

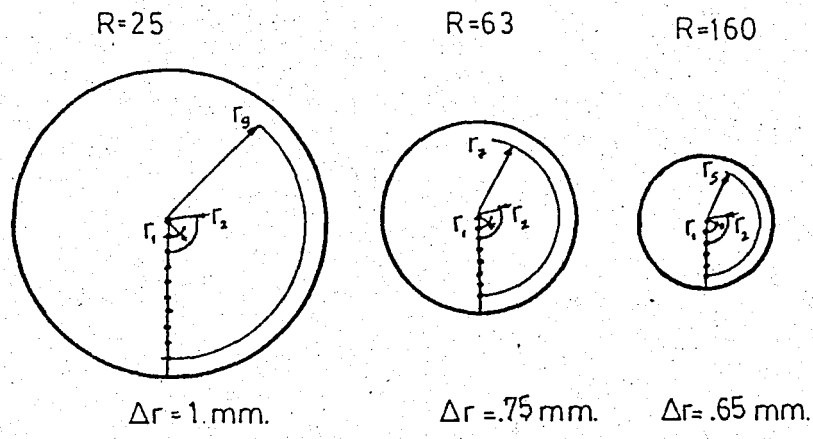

FIGURE 22. Measurement places to determine the hardness.

Microhardness tests performed fall into three categories. Purpose of the first serial tests was to determine the variation of microhardness with initial billet temeprature and extrusion ratio. Nine specimens which were extruded at 350,400 and 450°C initial billet temperature with the extrusion ratios of 25:1, 63:1 and 160:1, were tested. To test the rods at same conditions for different extrusion ratios, all specimens were chosen from the middle of the rods.

Second serial tests were performed to examine the hardness variation along the rods. Specimens were cut from the A,B and C positions of the rods(Fig.23).

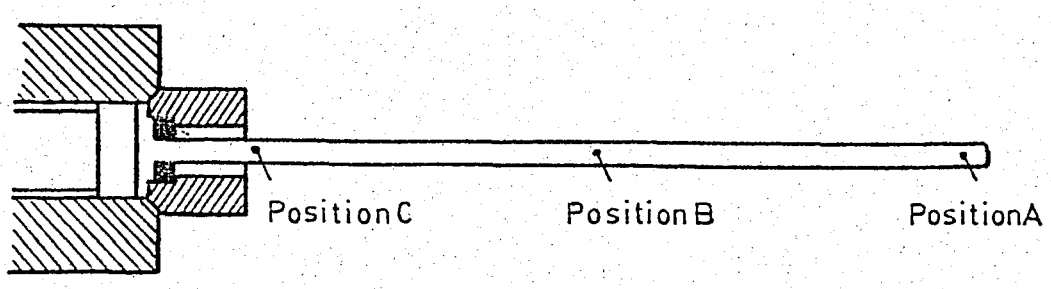

FIGURE 23. Measurement places to determine the hardness variation along the rods.

Third serial tests determined the microhardness variation throughout the diameter of the products which have the fibrous structures.

4. Tension Tests

Tension tests were performed by means of an Instron-1115 test equipment (Fig.24).Specimens for tension tests were cut from the middle of the rods which were extruded at 350, 400, 450^{o}C initial billet temperatures with the extrusion ratios of 25:1, 63:1 and 160:1, and prepared according to TS 138 standart (Fig.25).A typical graph obtained from the tension test is given in Fig.26. In all of the tension tests, the speed of crosshead was chosen to be 0.2 cm/min. Considering that ther are no apperant yield point in the graphes of load-elongation, (Fig.26) proof stresses were determined by means of the extension-under-load method according to the method of

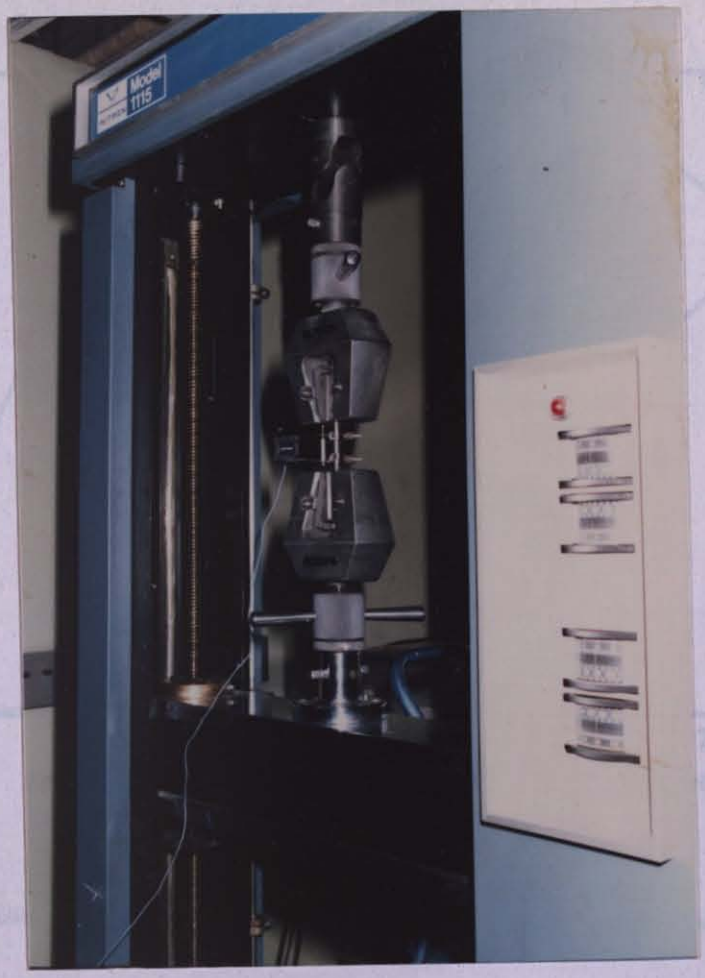

FIGURE 24. Instron-115 tension test equipment .

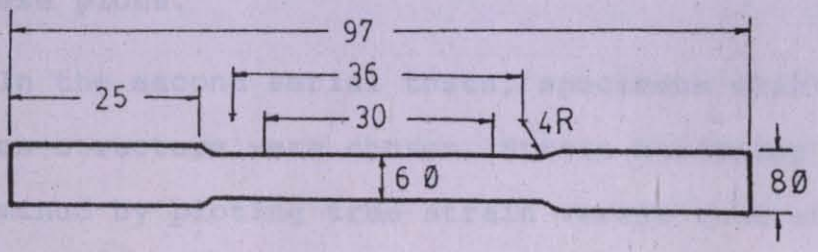

FIGURE 25. TS 138-6 Tension test specimen .

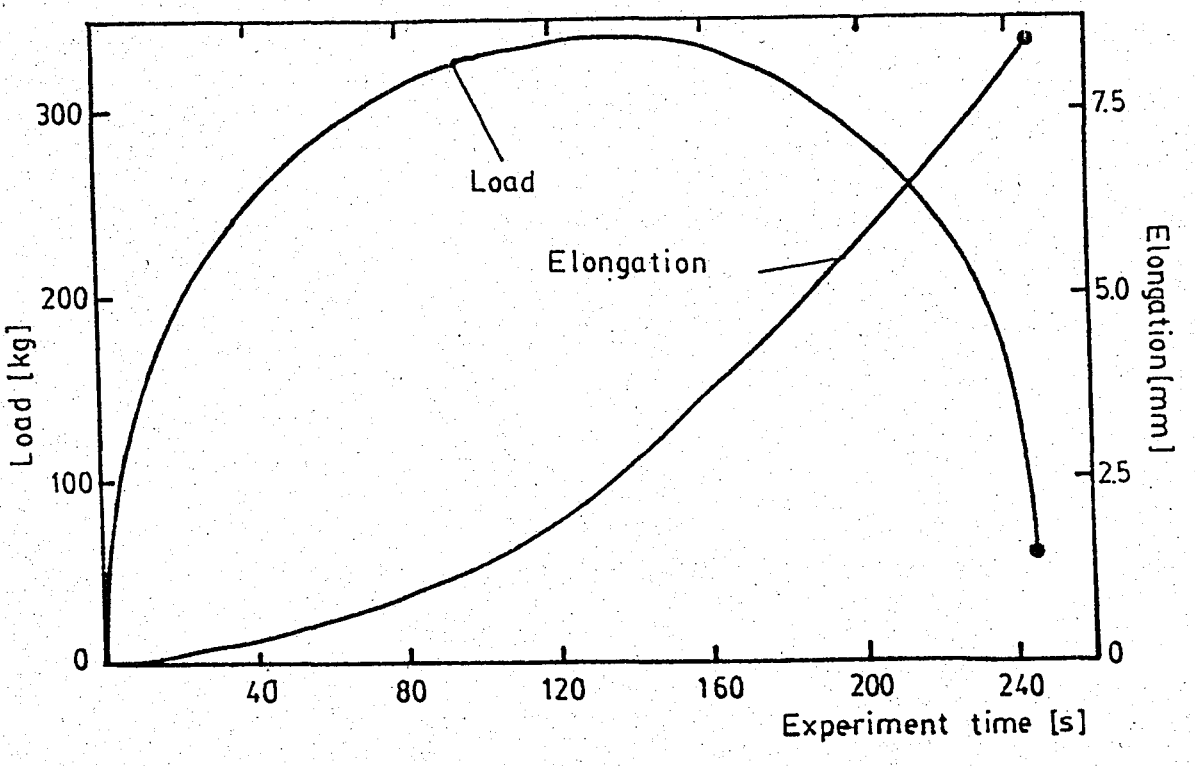

FIGURE 26. Typical elongation and load curves obtained from tension test.

ASTM E-8 standard specified extension-under-load was determined to be 0.23 % by ploting the stress-strain curves and averaging plastic strain values corresponding to elastic strain of 0.2% in these plots.

In the second serial tests, specimens which have only fibrous structure were chosen. Strain hardening exponent was determined by ploting true strain versus true stress curve in logarithm scale and calculating the slope of the curve after yielding.

B- EXPERIMENTAL RESULTS

1. Microstructure

Variation of recrystallized grain size with the temperature corrected strain rate, Z_i is given in Figs.27 and 28. Temperature corrected strain rate was calculated by

$$Z_i = \dot{\varepsilon} \cdot \exp\left(\frac{\Delta H}{G.T_o}\right) \qquad (26)$$

where T_o is initial billet temperature. Activation energy. ΔH was been given for this process

$$\Delta H = 156.5 \text{ kj/mol} \qquad (27)$$

in the literature [3]. Strain rate, $\dot{\varepsilon}$ was calculated by Eq.2

Lineal intercept method [31] was used to estimate the grain size,d. The number of grains intercepted by three straight lines was counted on the photomicrographs of a representative field of the specimens cut from the rods which were extruded at 350,400 and 450°C initial billet temperatures with the extrusion ratios of 25:1 and 160:1.Fig.27 and Fig.28 show the variation of the recrystallized grain size with the temperature corrected strain rate, Z_i, for R=25 and R=160 respectively.

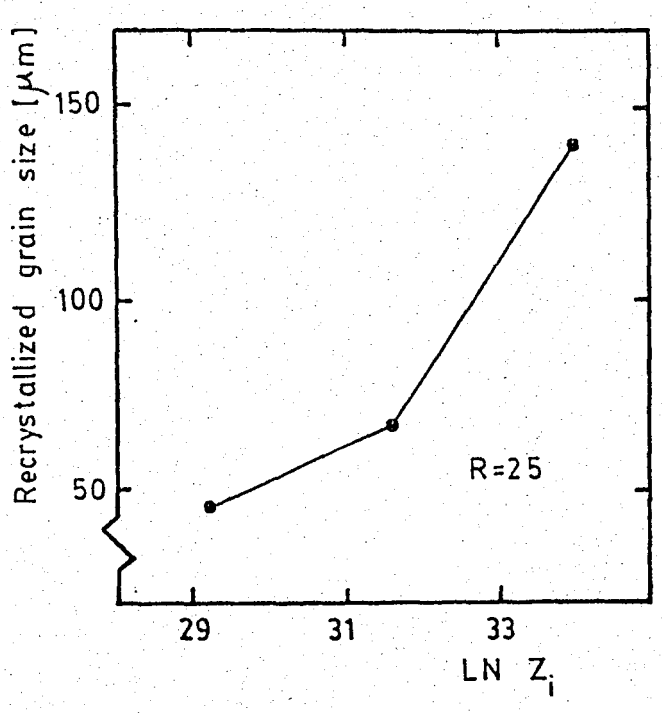

FIGURE 27. Variation of recrystallized grain size with the logarithm of Z_i for R=25 .

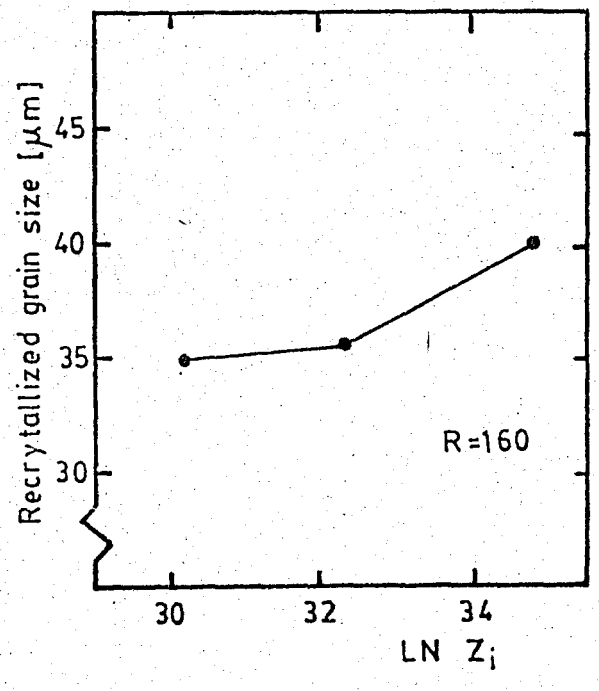

FIGURE 28. Variation of recrystallized grain size with the logarithm of Z_i for R=160.

Photomicrographs of the products which were extruded with an extrusion ratio of 25:1 at 350°C, 400°C and 450°C initial billet temperatures are given in Figs 29,30 and 31. Figure 29 shows a fibrous structure, while Figs.30 and 31 show dublex structure. Figures 32 and 33 show the microstructure of products which were extruded with an extrusion ratio of 63:1 at 350°C and 400°C initial billet temperatures. Both of them show dublex structure. Photomicrographs given in Figs.29-33 have a magnification of about 50:1.

FIGURE 29. Microstructure of the product which was extruded with an extrusion ratio of 25:1 at 350°C initial billet temperature.

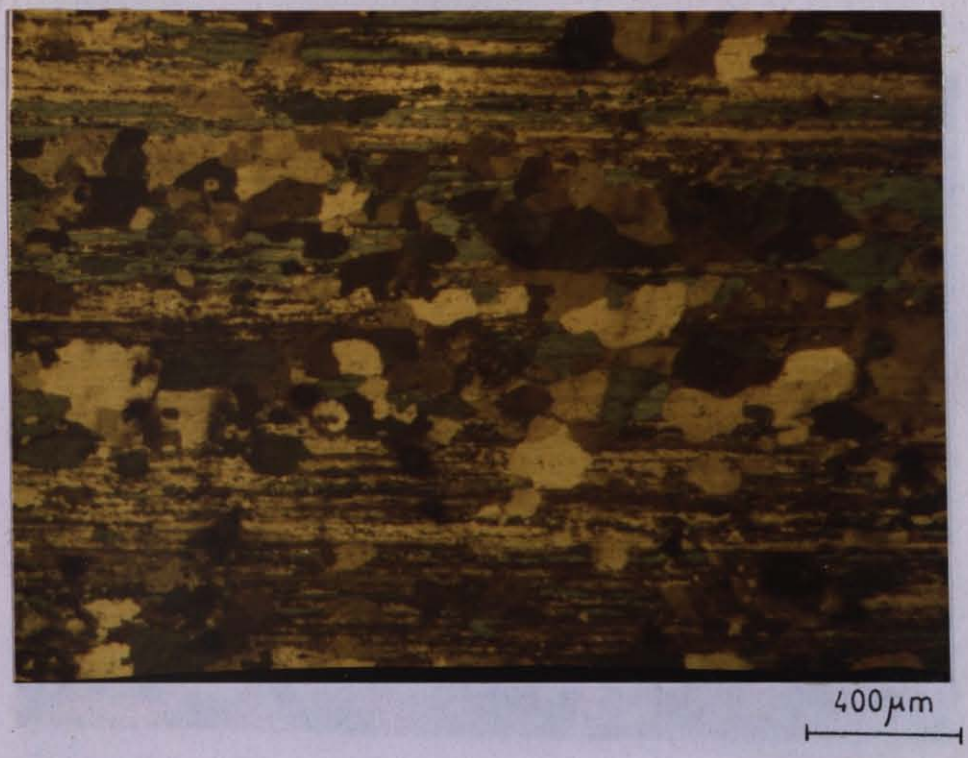

FIGURE 30. Microstructure of the product which was extruded with an extrusion ratio of 25:1 at 400°C initial billet temperature.

FIGURE 31. Microstructure of product which was extruded with an extrusion ratio of 25:1 at 450 °C initial billet temperature.

FIGURE 32. Microstructure of product which was extruded with an extrusion ratio of 63:1 at 350°C initial billet temperature.

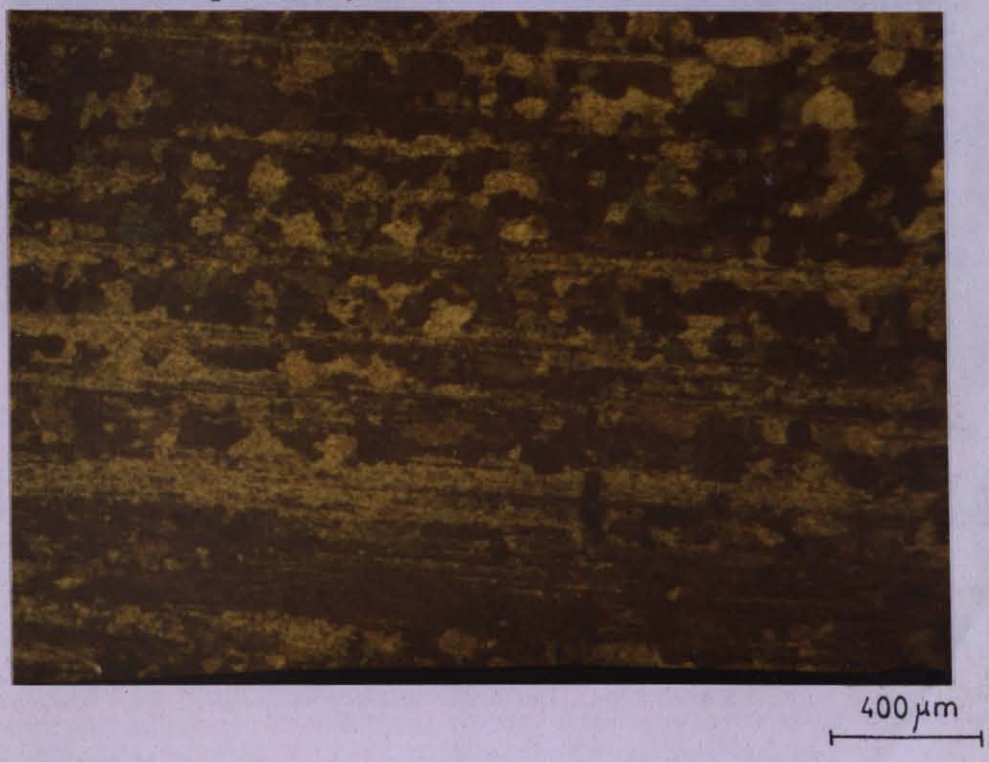

FIGURE 33. Microstructure of product which was extruded with an extrusion ratio of 63:1 at 400°C initial billet temperature.

Photomicrographes of the products which were extruded with an extrusion ratio of 160:1 at 350°C, 400°C and 450°C initial billet temperatures are given in Figs. 34,35 and 36. Figs.34 and 35 show the dublex structures, while Fig.36 show a fully recrystallized structure. Photomicrographes given in Figs. 34-36 have a magnification of 200:1. Some other photomicrographes of the extruded products are given in Appendix C.

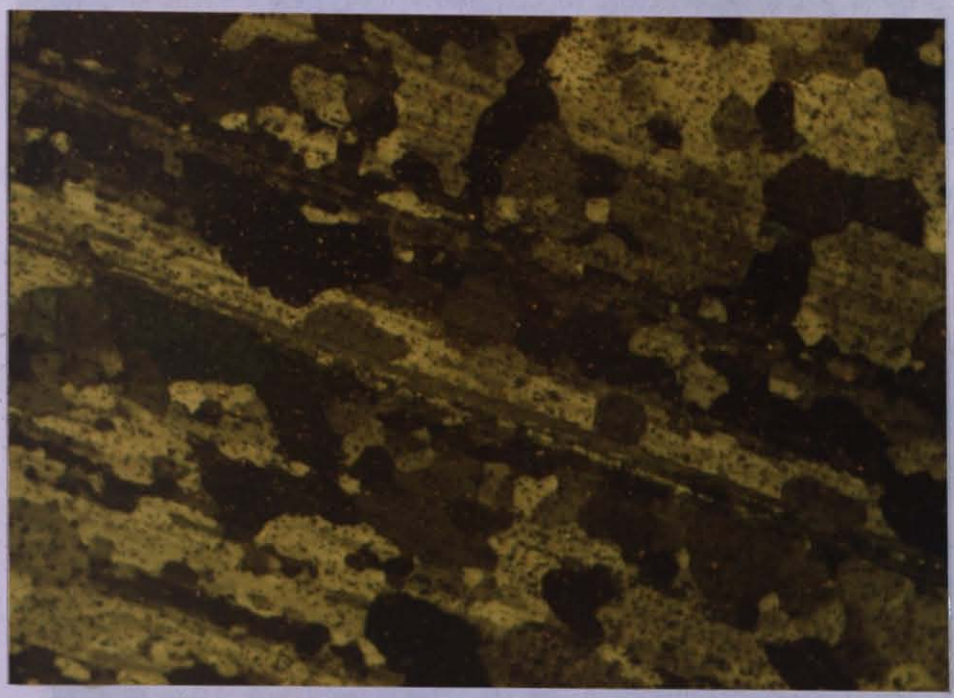

FIGURE 34. Microstructure of the product which was extruded with an extrusion ratio of 160:1 at 350°C initial billet temperature.

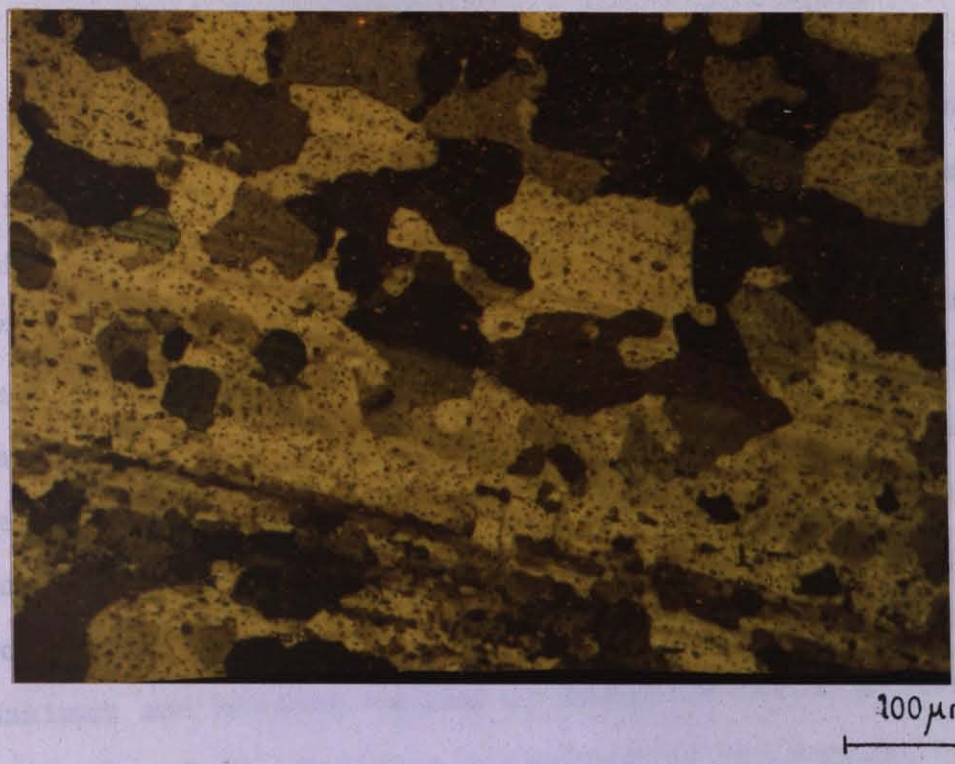

FIGURE 35. Microstructure of the product which was extruded with an extrusion ratio of 160:1 at 400°C initial billet temperat

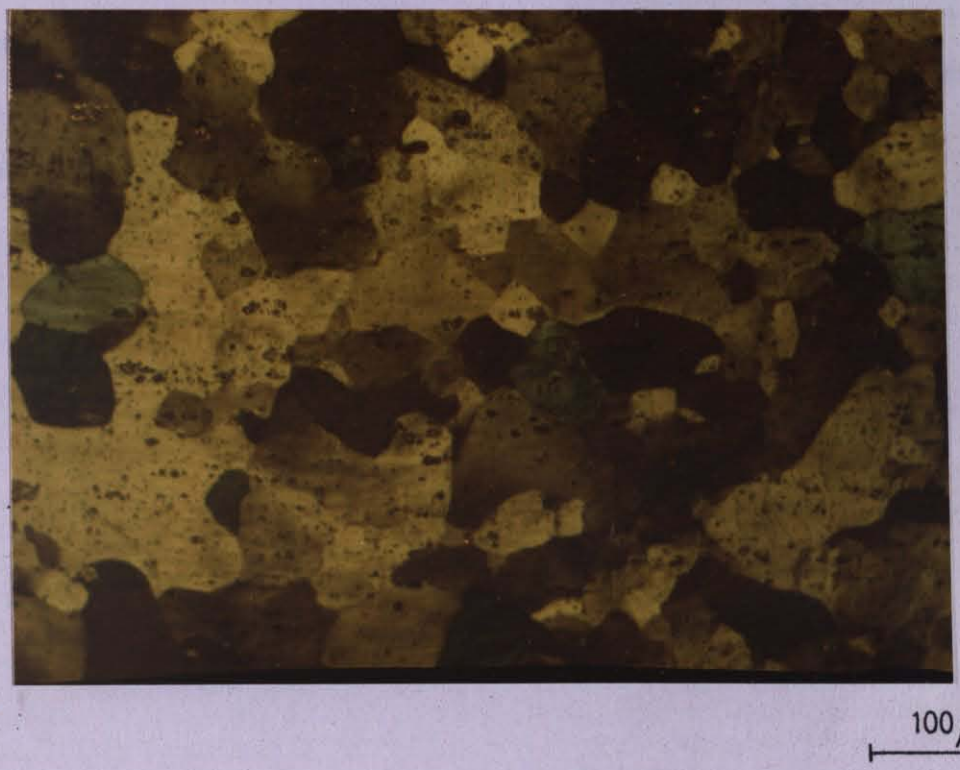

FIGURE 36. Microstructure of the product which was extruded with an extrusion ratio of 160:1 at 450°C initial billet temperature.

2. Mechanical Properties

Results of microhardness tests are tabulated in Tables 2 3 and 4 according to the positions from where specimens were taken. Position B represents the middle position of the rods (Fig.23). Since the temperature rise during the extrusion depends on the length of product, the variation of average hardness of the product with extrusion ratio and initial billet temperutare are plotted according to Position B. Microhardness measurements were performed 6-10 different places across the section represented by r_o-r_{10} as given in Fig.22. Maximum and minimum values of hardness are also given in Figs.37 and 38. Position A represents the beginning position of the rods while position C represents the end position. (Fig.23) Fig.39 shows the variation of hardness with the position along the products. It should be noted that, in this graph, maximum values of the hardness across the section were considered.

TABLE 2. Results of microhardness tests performed on the specimens cut from Position B .

R	T_o [^oC]	Places where microhardness tests were performed										VS (average)
		r_o	r_1	r_2	r_3	r_4	r_5	r_6	r_7	r_8	r_9	
25	350	41.1	38.5	37.0	38.4	37.6	36.9	37.0	35.4	36.6	34.5	37.3
25	400	40.4	39.1	38.8	38.8	36.1	35.9	37.2	35.4	36.2	36.9	37.5
25	450	50.4	44.4	43.4	42.7	40.6	43.6	44.0	38.6	40.9	40.2	42.9
63	350	39.2	38.1	36.8	34.9	35.2	37.1	37.7	36.9			37.0
63	400	45.2	42.2	40.4	43.8	44.3	40.9	43.9	44.4			43.1
160	350	41.4	44.5	35.5	36.6	37.3	39.7					39.2
160	400	46.5	44.1	39.6	42.7	41.7	43.8					43.1
160	450	58.4	54.9	53.6	53.4	51.3	65.9					56.3

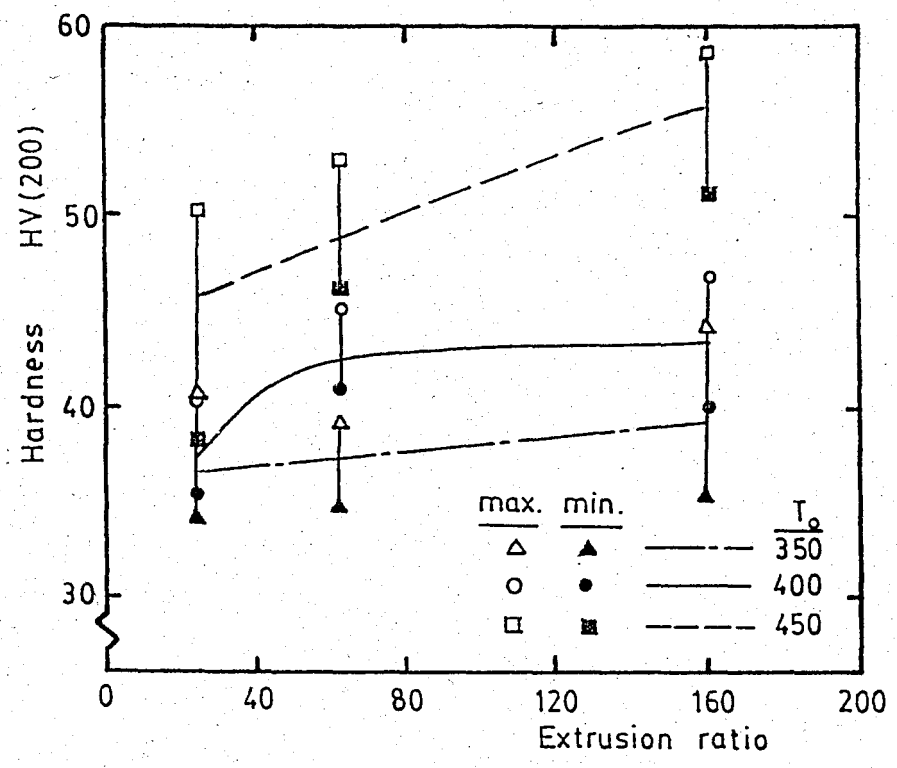

FIGURE 37. Variation of hardness with the extrusion ratio.

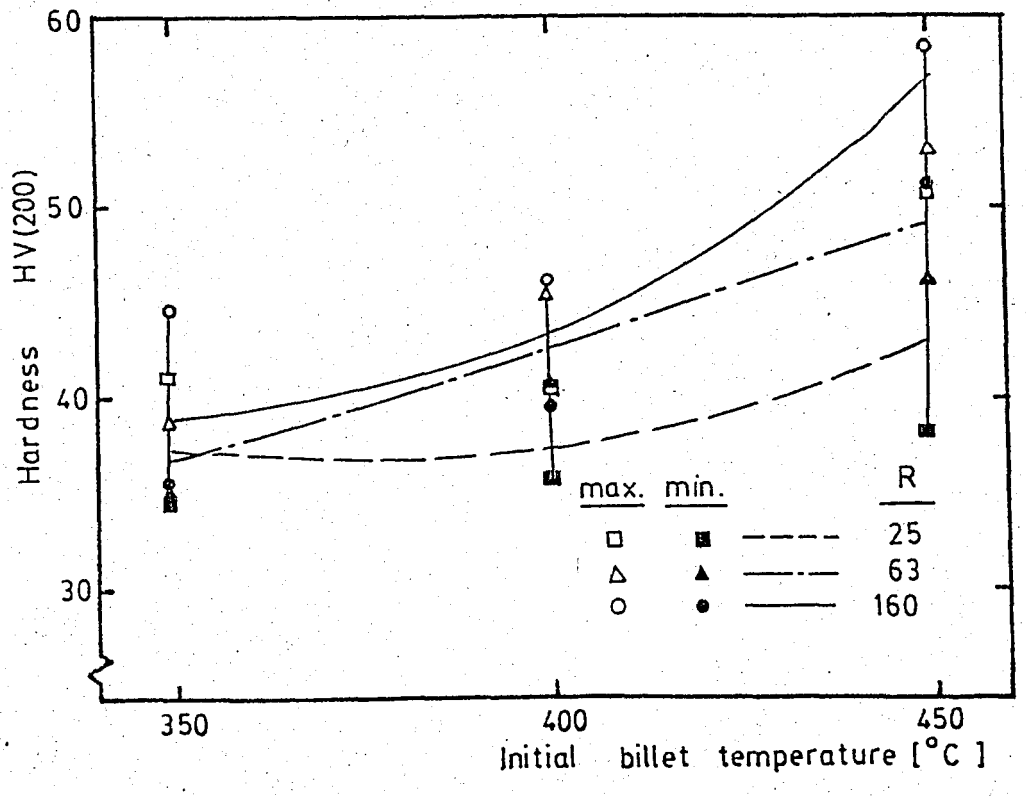

FIGURE 38. Variation of hardness with the initial billet temperature

TABLE 3. Results of microhardness tests, performed on the specimens cut from position A.

R	T_o [^oC]	Places where microhardness test were performed										VS (Average)
		r_o	r_1	r_2	r_3	r_4	r_5	r_6	r_7	r_8	r_9	
25	350	51.8	50.8	50.7	48.4	47.5	45.9	44.6	43.4	42.9	42.7	46.9
25	450	47.9	45.6	44.4	44.3	43.7	42.5	42.3	42.1	41.9	39.9	43.5
63	400	49.6	48.7	48.3	48.4	47.6	47.4	46.4	40.7			47.1
160	400	45.2	42.5	41.6	43.8	42.3	40.5					42.7

TABLE 4. Results of the microhardness tests, performed on the specimens cut from Position C.

R	T_o [°C]	Places where microhardness tests were performed										VS (Average)
		r_o	r_1	r_2	r_3	r_4	r_5	r_6	r_7	r_8	r_9	
25	350	48.1	49.8	45.8	41.3	39.7	39.7	46.3	43.5	42.9	45.7	44.4
25	400	46.8	43.0	41.1	43.6	41.0	39.4	37.0	38.6	42.7	41.9	41.5
25	450	57.9	53.8	50.6	51.6	51.3	47.3	50.3	46.7	45.0	47.3	50.2
63	400	46.4	43.5	46.4	43.7	43.4	45.4	45.3	45.4			44.9
160	400	46.7	45.5	46.4	44.3	44.5	42.9					45.0

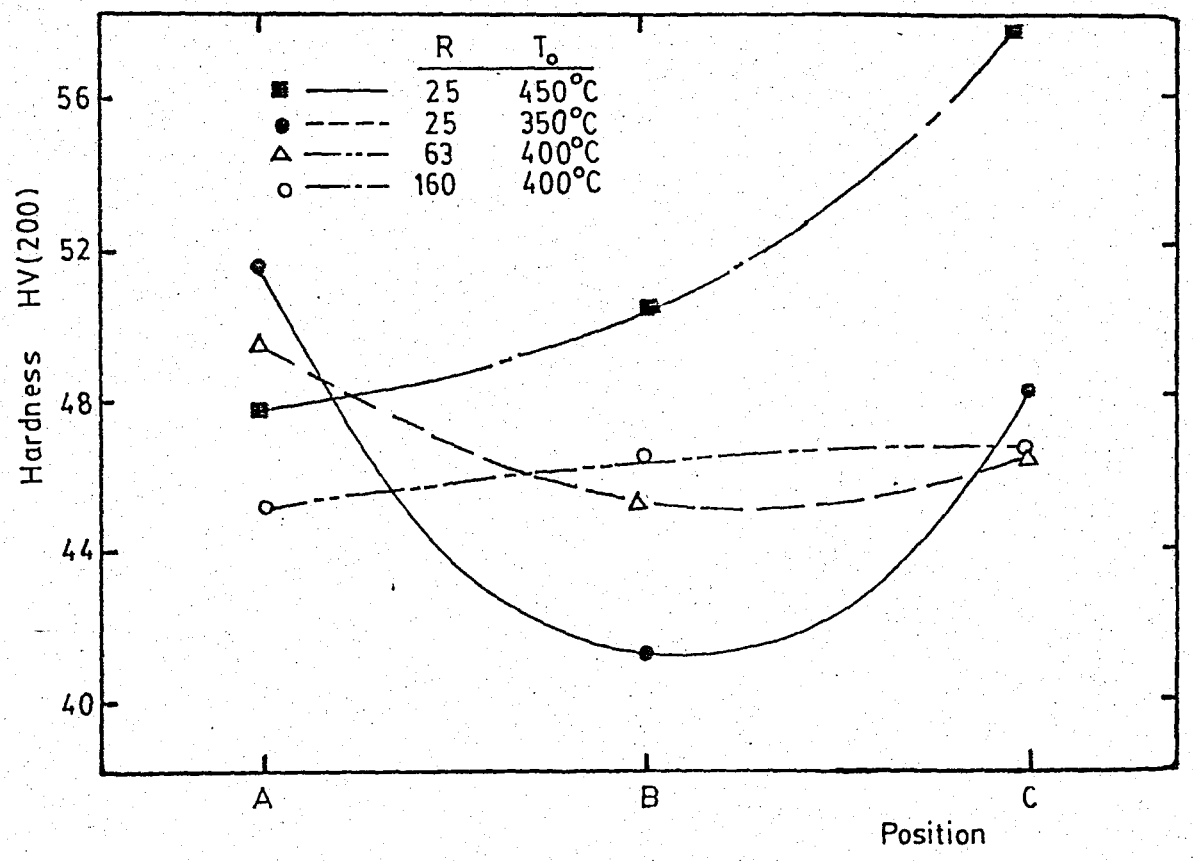

FIGURE 39. Variation of maximum microhardness values taken throughout the diameter with the position along the rod.

In Fig.40 variation of hardness throughout the diameters of the products, which were extruded at 350 and 450 °C initial billet temperatures with an extrusion ratio of 25:1, is illusturated for Position A. Metallographic examinations showed that these specimens have fibrous structure, showing that the only operative mechanism on the structure during and after extrusion is dynamic recovery.

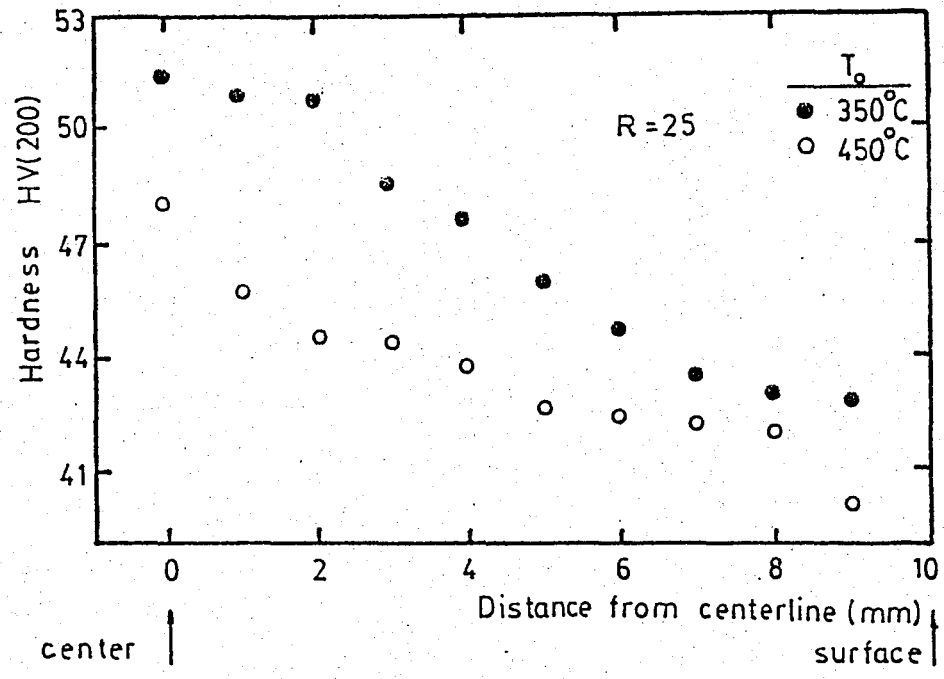

FIGURE 40. Variation of hardness with the distance from the centerline of the product.

In Fig.41, variation of hardness with the logarithm of the strain rates corresponding to the positions shown in Fig.22 is shown. The strain rate values were calculated by means of a computer programme. Detailed information about this programme is given in Appendix B.

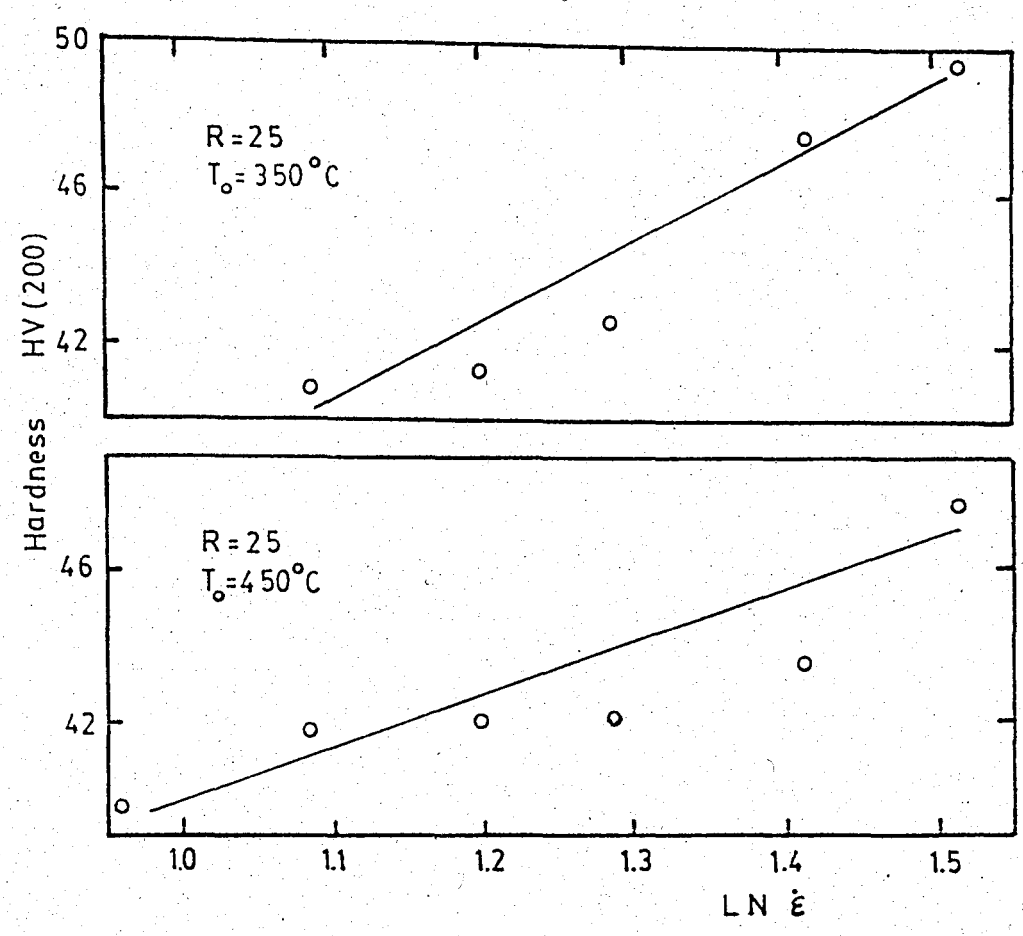

FIGURE 41. Dependence of hardness on the logarithm of strain rate for constant temperature .

Proof stress, $\sigma_{0,2}$, ultimate tensile strength, σ_{UTS} and final strain data are given in Table 5. These data were obtained from the tension tests, performed on the specimens cut from the rods which were extruded at 350,400 and 450°C initial billet temperatures with the extrusion ratios of 25:1, 63:1 and 160:1.

TABLE 5. Proof stress, $\sigma_{0.2}$, ultimate tensile strength, σ_{UTS} and final strain values obtained from tenison tests.

T_o	350 °C			400 °C			450 °C		
R	$\sigma_{0.2}$ [MPa]	σ_{UTS} [MPa]	Final Strain %	$\sigma_{0.2}$ [MPa]	σ_{UTS} [MPa]	Final strain %	$\sigma_{0.2}$ [MPa]	σ_{UTS} [MPa]	Final strain %
25	66.1	115.0	26.3	63.8	124.5	27.3	59.7	119.4	30.7
63	62.8	116.0	27.7	52.6	105.7	28.7	48.6	100.6	31.3
160	73.4	147.1	24.7	55.2	112.2	26.7	56.0	124.4	27.0

Variations of proof stress, ratio of proof stress to ultimate tensile strength and final strain with initial billet temperature are given in Figs 42,43 and 44, respectively. Proof stress, ratio of proof stress to ultimate tensile strength and final strain are also plotted against the extrusion ratio. These are given in Figs.45,46 and 47, respectively It should be noted that the tension test specimens were cut from the position B of products and designed according to TS 138, and data obtained from the tests were evaulated according to ASTM. E-8.

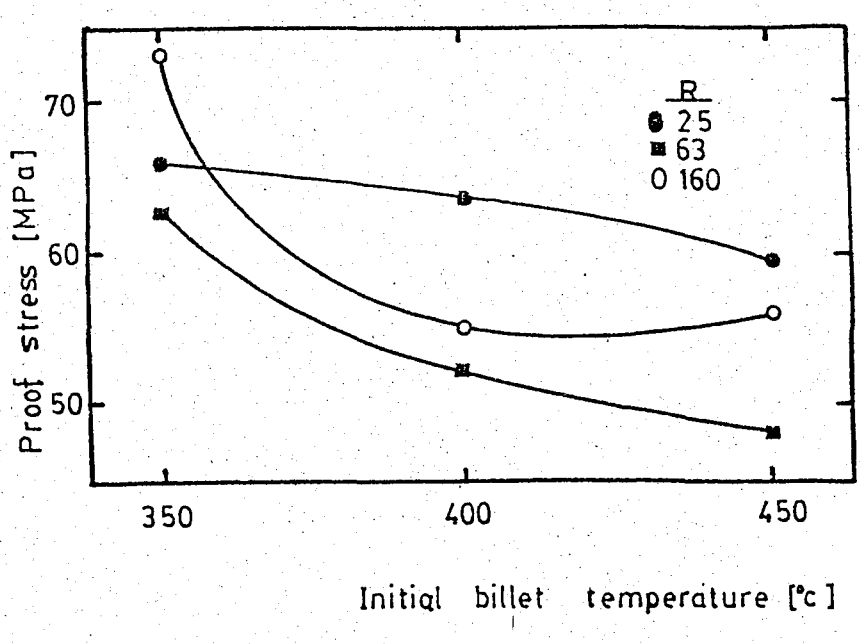

FIGURE 42. Variation of proof stress with initial billet temperature.

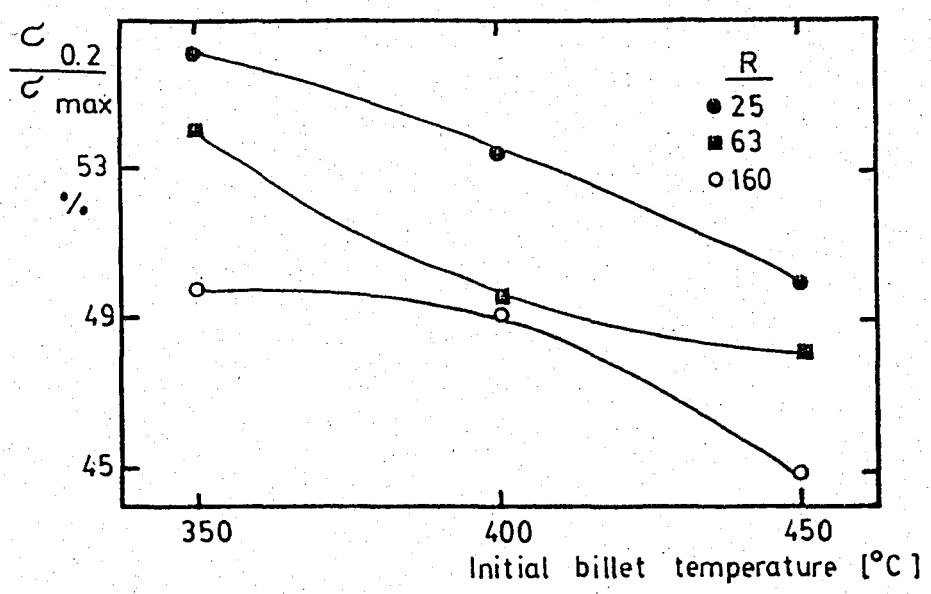

FIGURE 43. Variation of the ratio of proof stress to ultimate tensile strength with initial billet temperature.

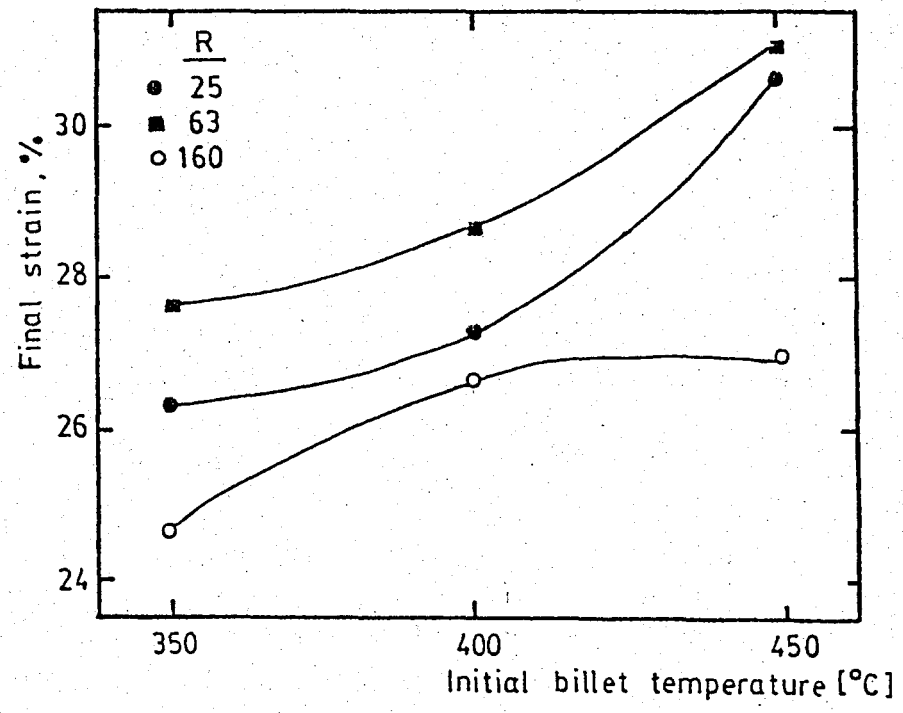

FIGURE 44. Variation of final strain with initial billet temperature.

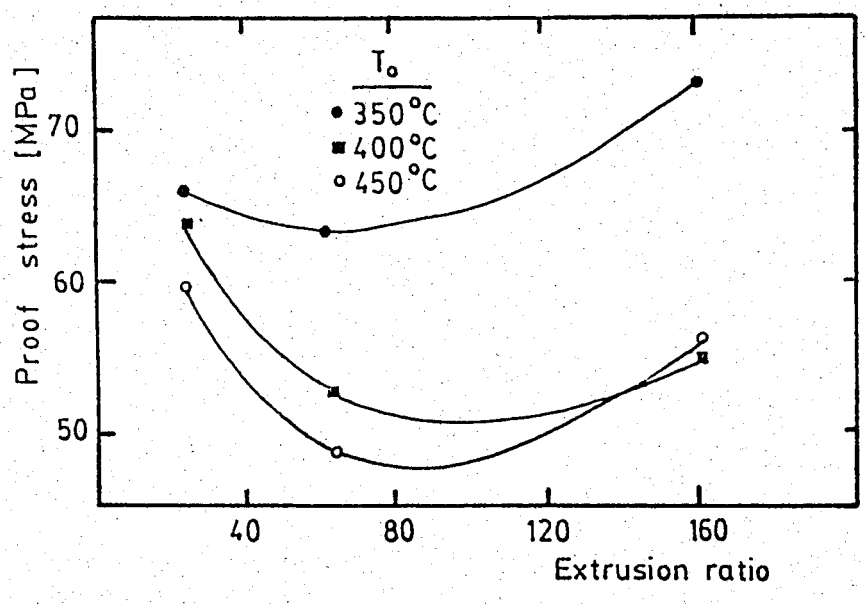

FIGURE 45. Variation of proof stress with extrusion ratio.

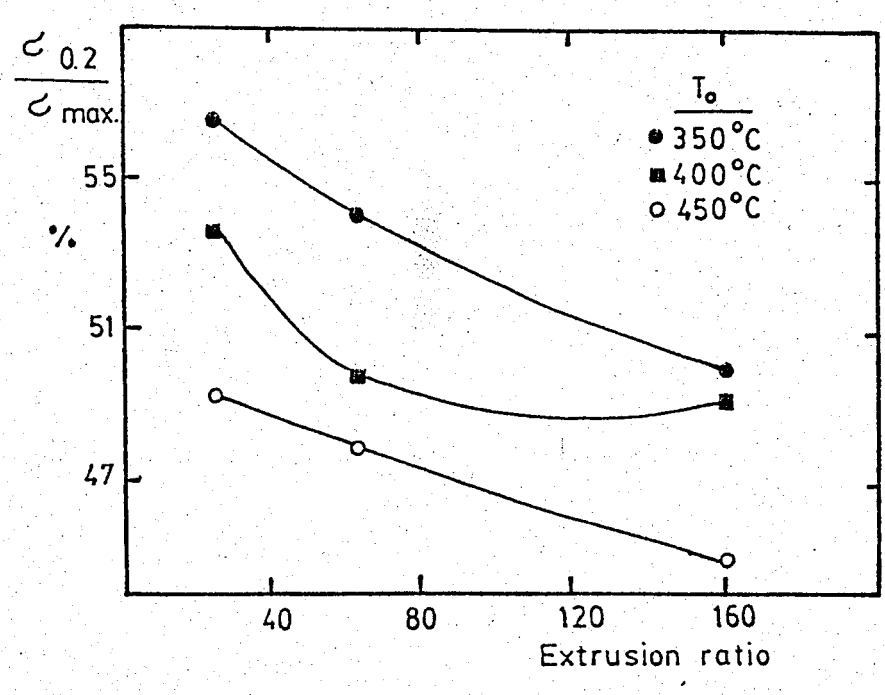

FIGURE 46. Variation of the ratio of proof stress to ultimate tensile strength with extrusion ratio.

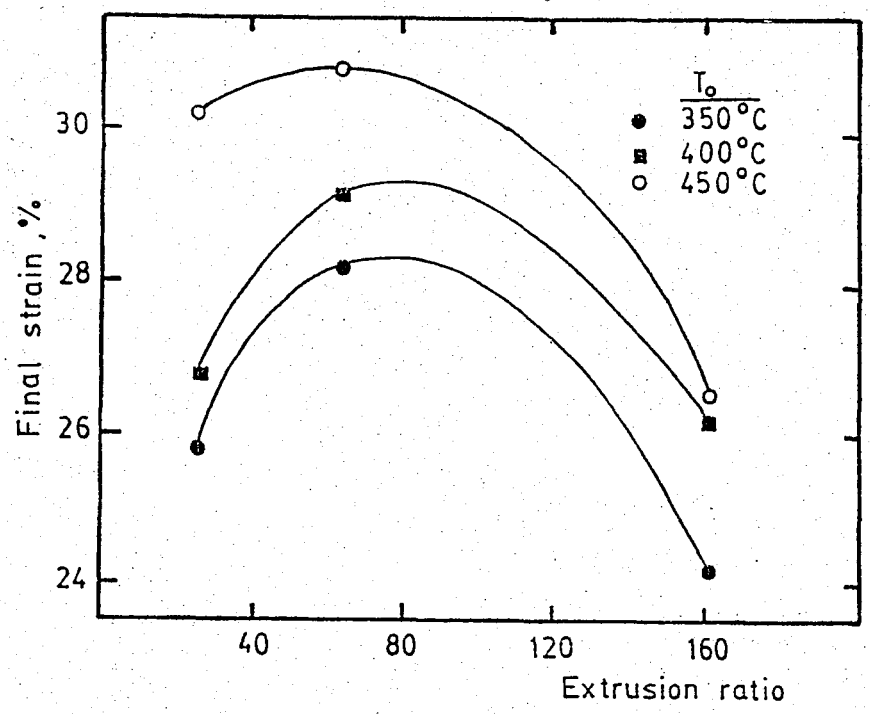

FIGURE 47. Variation of final strain with extrusion ratio.

Results of second serial tension tests, performed on the rods which were observed to have only fibrous structure by metallographic examinations, are given in Table 6. Data obtained from these tests were evaluated and proof stress, strain hardening exponent and ultimate tensile strength were plotted against the logarithm of temperature corrected strain rate. These graphes are given in Figs. 48,49 and 50. Temperature corrected strain rate was calculated by the equation

$$Z = \dot{\varepsilon} \cdot \exp\left(\frac{\Delta H}{GT}\right) \qquad (8)$$

TABLE 6. Proof stress, $\sigma_{0.2}$ ultimate tensile strength, σ_{UTS} and strain hardening exponent, n values obtained from tension tests performed on specimens which have fibrous structure.

No	$T_o[^oC]$	R	$T[^oC]$	$\dot{\varepsilon}[s^{-1}]$	LnZ	$\sigma_{0.2}$	σ_{UTS}	n
1	350	25	355	4.49	31.48	66.7	113.3	0.130
2	350	25	361	4.45	31.18	65.9	114.4	0.137
3	350	25	383	4.41	30.18	64.5	118.0	0.150
4	400	63	430	11.36	29.21	62.6	123.6	0.182
5	450	63	455	11.36	28.28	61.6	119.9	0.200
6	450	25	455	4.49	27.36	59.7	126.0	0.219

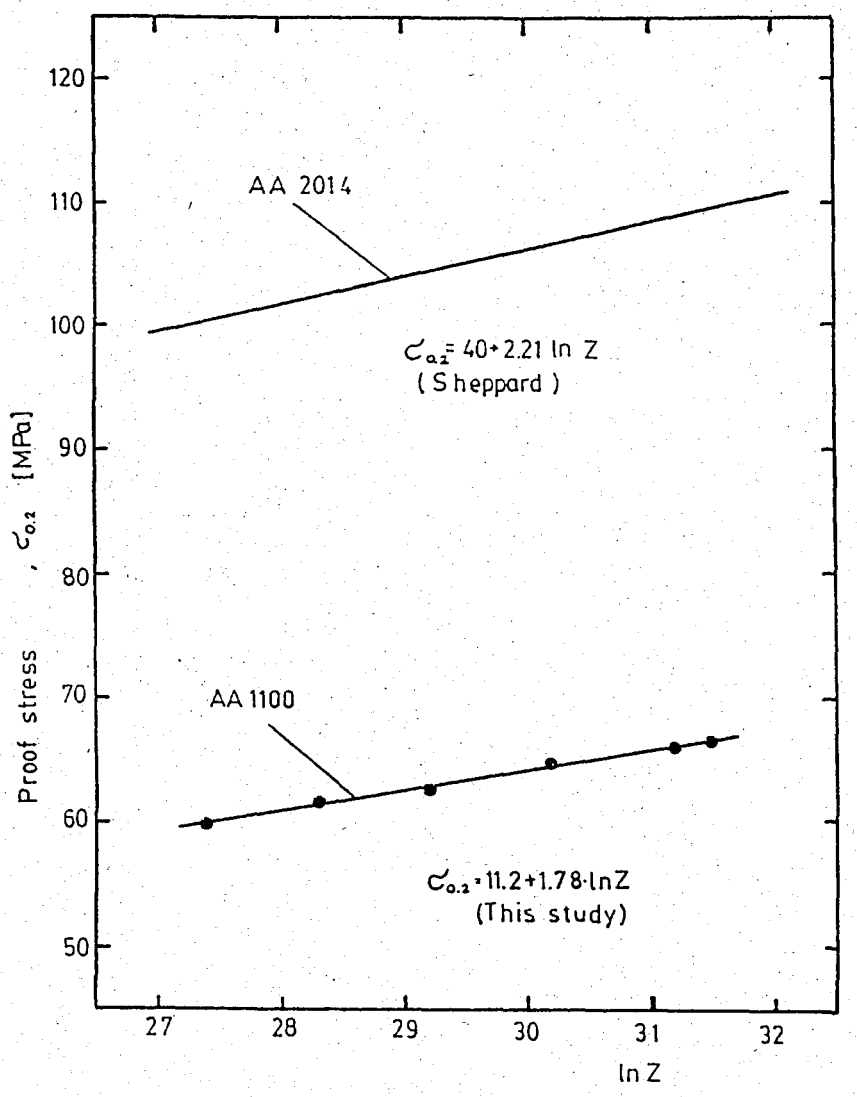

FIGURE 48. Variation of proof stress with the temperature corrected strain rate.

In this equation, deformation temperature, T was determined from the temperature rise curves as shown in Fig.5, considering the length of product where the specimens were cut. Mean strain rate, $\dot{\varepsilon}$ was calculated by averaging the strain rate values inside the specimen diameter, calculated by the computer programme mentioned in Chapter 2.

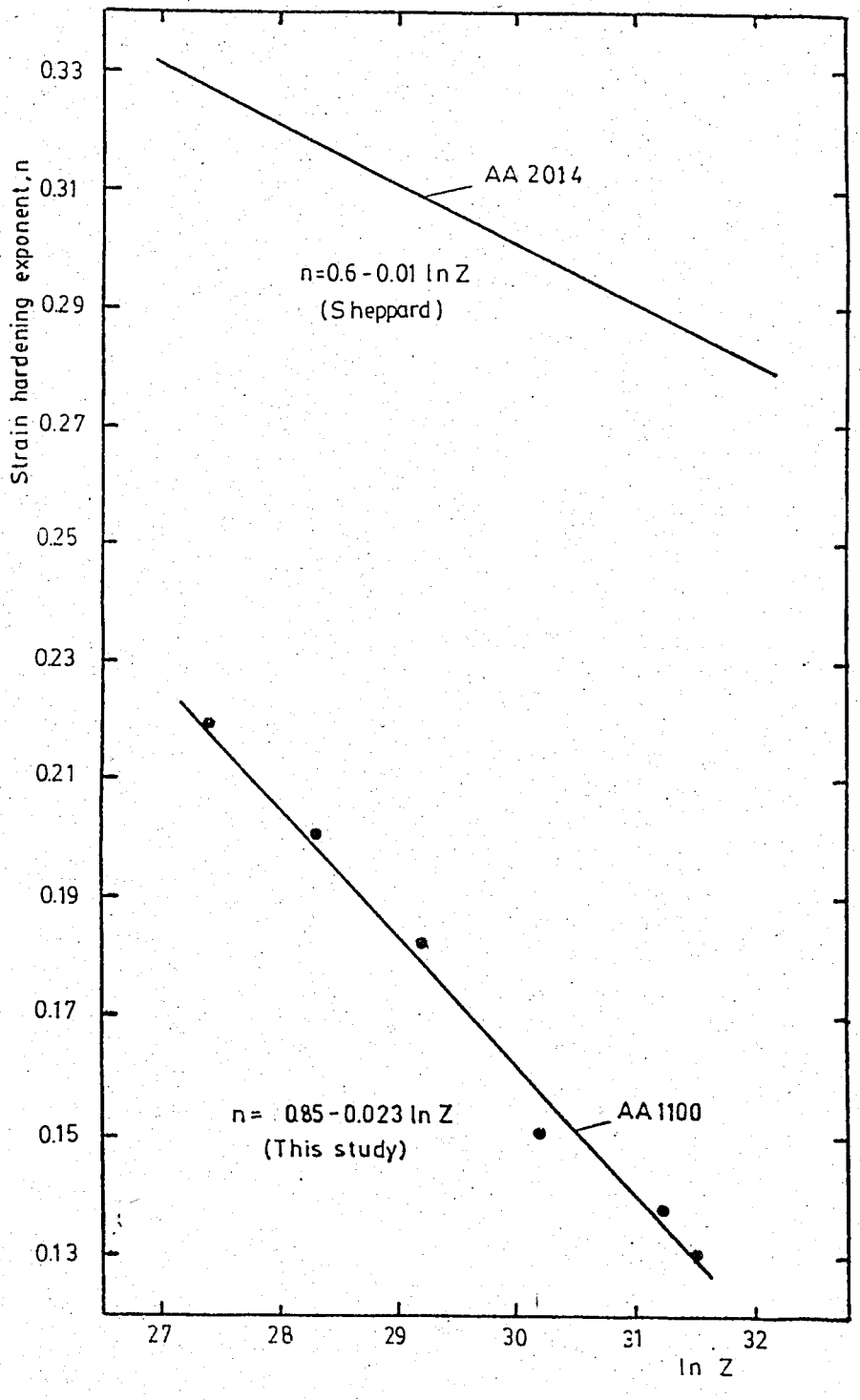

FIGURE 49. Variation of strain hardening exponent with the logarithm of temperature corrected strain rate.

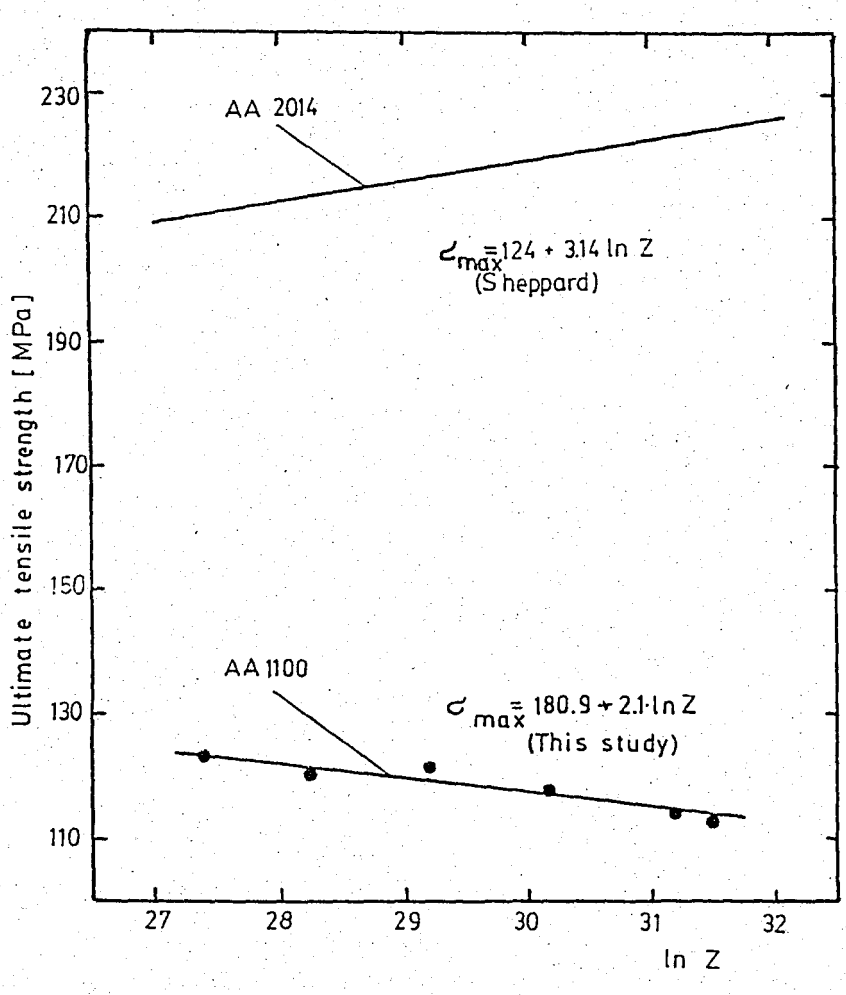

FIGURE 50. Variation of ultimate tensile strength with the logarithm of temperature corrected strain rate.

IV. DISCUSSION OF THE RESULTS

A. MICROSTRUCTURE

Metallographic examinations show that three types of structure appear in product; fibrous structure as shown in Fig.51.a, dublex structure as shown in Fig.51.b, fully recrystallized structure as shown in Fig.51.c. Although, this is in aggrement with most previous workers[5-15], it has been reported that, for water quenching, fibrous structure appears mostly. For same working conditions, but air-cooling,fibrous structure appeared only in the products which were extruded at 350^{o}C initial billet temperature. Since, the products are subjected to high temperature for a longer duration than in water-quenching conditions, this is not surprising.

Fig.27 and 28 shows that, for constant extrusion ratio, increasing temperature leads to an increase in the diameter of recrystallized grains as reported by previous authors [21]. Although dynamic recovery is usually the mechanism operative during the deformation, the strain, strain rate and temperature conditions may be suitable to provide the driving force

for static recrystallization. Since these properties cannot be determined accurately, structural changes across the section are difficult to determine. Except these inner locations, it was

T_o = 350 °C
R = 25
length of product, L=10cm.

T_o = 400 °C
R = 25
L = 200 cm.

T_o = 450°C
R = 160
L = 400 cm.

FIGURE 51. Microstructures of extruded products a) fibrous b) dublex, and c) fully recrystallized structure.

observed that recrystallization begins at the surface of products, as reported by most previous workers [6]. This may be because of the strain rate which has a minimum value at the surface. Amount of recrystallized locations increases with the initial billet temperature for constant extrusion ratio, as shown in Figs. 34,35 and 36.

Another result which is in agreement with previous authers [21] is that, for constant initial billet temperature, recrystallized grain size increases with decreasing extrusion ratio. This can be seen in Figs. 30,33 and 35. Reason for this happening is the increasing strain rate due to the increasing extrusion ratio.

B. MECHANICAL PROPERTIES

The effects of extrusion ratio and initial billet temperature on the hardness of product are shown in Figs. 37 and 38. It should be noted that, in these graphes, the dependence of temperature rise on the extrusion ratio was not considered.

Sheppard [6] has noted that mechanical properties of product increase with the increasing temperature corrected strain rate. The hardness of product increases with increasing extrusion ratio as shown in Fig.37, supporting the Sheppard's conclusions, since the increase in strain rate, due to the increasing extrusion ratio, results in increase of the temperature corrected strain rate via the Eq.8. But hardness of product also increases with increasing initial billet temperature, although temperature corrected strain rate decreases

with increasing temperature as shown in Fig.38. This result is not in agreement with Sheppard. The fine precipitates may be reason of this result as reported by previous authers [21].

Although, the hardness value across the section varies in a large range, it takes the maximum value around the centerlines, so, instead of average hardness, these maximum values were taken into acccount to compare the results. The results of tests performed for examining the hardness variations along the rods are in agreement with the assumption that temperature corrected strain rate may be effective until a critical point is reached after which precipitation is more effective. As shown in Fig. 39, hardnesses of the products with 25:1 extrusion ratio at 350°C and 63:1 extrusion ratio at 400°C decrease from position A of the product to position B then, after a critical point, begin to increase. However, for 160:1 extrusion ratio at 400 °C and 25:1 extrusion ratio at 450°C products, this critical point may be reached initially and the hardnesses of these products increase along the rods.

For some products, hardness values throughout the diameter are maximum at the centerlines of the rods and decrease as the distance from the centerline increases, as shown in Fig.40. As a result of metallographic examinations, it was observed that most of these specimens had only fibrous structure, indicating that dynamic recovery was operative mechanism. Assuming that the temperature is constant across the section, one can see that this variation of hardness may be related to the strain rate. The hardness values were plotted against the

logarithm of strain rate corresponding to the points where hardness measurements were taken (Fig.41). Regressions resulted in the linear relationships.Considering the slopes of lines in Fig.41, it can be seen that dependence of hardness on the strain rate decreases with increasing deformation temperature.

When the values of proof stress and final strain are plotted versus the initial billet temperature in Figs. 42 and 44, we can see that increasing billet temperature causes increases in final strain and decreases in proof stress. These effects of initial billet temperature on the final strain and proof stress are in agreement with previous papers [6,19]. However, the effects of this process parameters on the ratio of proof stress to ultimate tensile strength have not been reported in the literature. As shown in Fig.43, the ratio of the proof stress to ultimate tensile strength increases with the increasing initial billet temperature. This may be related to the strain hardening exponent. For commercial pure aluminum, it has been reported that temperature rise leads to finer precipitation in the matrix [21]. This may be reason for the increase in the strain hardening exponent. Effects of extrusion ratio on the mechanical properties of product are shown in Figs. 45-47. The influence of the extrusion ratio on the temperature rise makes these results difficult to analyse.

As a result of tension testing of the products which have only fibrous structure, strain hardening exponent, proof stress and ultimate tensile strength plotted against the logarithm of temperature corrected strain rate are shown in Figs.48-50. Regressions fitted the linear relationships :

$$\sigma_{0.2} = 11.2 + 1.78\ \mathrm{LnZ}\ [\mathrm{MPa}] \tag{28}$$

$$\sigma_{UTS} = 180.9 + 2.1\ \mathrm{LnZ}\ [\mathrm{MPa}] \tag{29}$$

$$n = 0.85 - 0.023\ \mathrm{LnZ} \tag{30}$$

Eq. 28 and Eq.30 are similar to those reported by Sheppard for AA2014 Alloy [6]. Dependence of strain hardening exponent on the temperature corrected strain rate for commercial pure aluminum is much more than that for AA2014, as we can see from the slope of the line in Fig.49. The reason for this may be, as mentioned before, the fine precipitates in the matrix.

Another interesting feature of commercial pure aluminum is that increasing temperature corrected strain rate leads to the decrease in ultimate tensile strength. But Sheppard has reported that ultimate tensile strength of AA2014 increases with this parameter. This different behaviour of commercial pure aluminum may be related to its strain hardening exponent.

Now, we can use these results in extrusion limit diagram as restricting conditions. We can state Eq.28 in the general form as

$$\sigma_{0.2} = A + B.\mathrm{LnZ} \tag{31}$$

Combining this equation with Eq.8

$$\sigma_{0.2} = A + B \cdot \frac{1}{T} + C\ \mathrm{Ln}\dot{\varepsilon} \tag{32}$$

recalling

$$\dot{\varepsilon} = \frac{6 . c . V . D_B^2 . \tan w}{D_B^3 - D_E^3} \qquad (2)$$

and for commercial pure aluminum

$$w = 54.1 + 3.45 \ \mathrm{Ln}R \qquad (3)$$

$$c = \mathrm{Ln}R \qquad (4)$$

we obtain

$$\dot{\varepsilon} = D \left(\frac{\mathrm{Ln}R \ . \ \tan (54.1 + 3.45 \ \mathrm{Ln}R)}{1 - \frac{1}{R\sqrt{R}}} \right) \qquad (33)$$

where D is a function of extrusion speed and billet diameter. Substituting Eq.33 into Eq.32 yields

$$\sigma_{0.2} = f \ (R,T) \qquad (34)$$

This implies that mechanical properties of the product can be expressed as a function of extrusion process parameters and taken into account in the extrusion limit diagram. Combining Eq.32 and Eq.33 and substituting constants of extrusion process for the experiments of this study into this equation, we obtain

$$\sigma_{0.2} = 9.06 + \frac{34.250}{T} + 1.78 \ \mathrm{Ln} \left(\frac{\mathrm{Ln}R . \tan (54.1 + 3.45 \ \mathrm{Ln}R)}{1 - \frac{1}{R\sqrt{R}}} \right) \qquad (35)$$

TABLE 7. Deformation temperature values corresponding to given extrusion ratios for specified proof stress values of product.

	Specified proof stress [MPa]			
R	50	55	60	65
4	586 °C	490 °C	414 °C	351 °C
9	597 °C	499 °C	421 °C	357 °C
16	602 °C	503 °C	424 °C	360 °C
25	606 °C	506 °C	426 °C	362 °C
169	615 °C	513 °C	432 °C	366 °C
400	617 °C	515 °C	433 °C	367 °C

By using this equation, deformation temperature values corresponding to given extrusion ratios were calculated for some specified proof stress values of product. These are given in Table 7 and were used to determine the curves shown in Fig.52. While proof stress values obtained from the tension

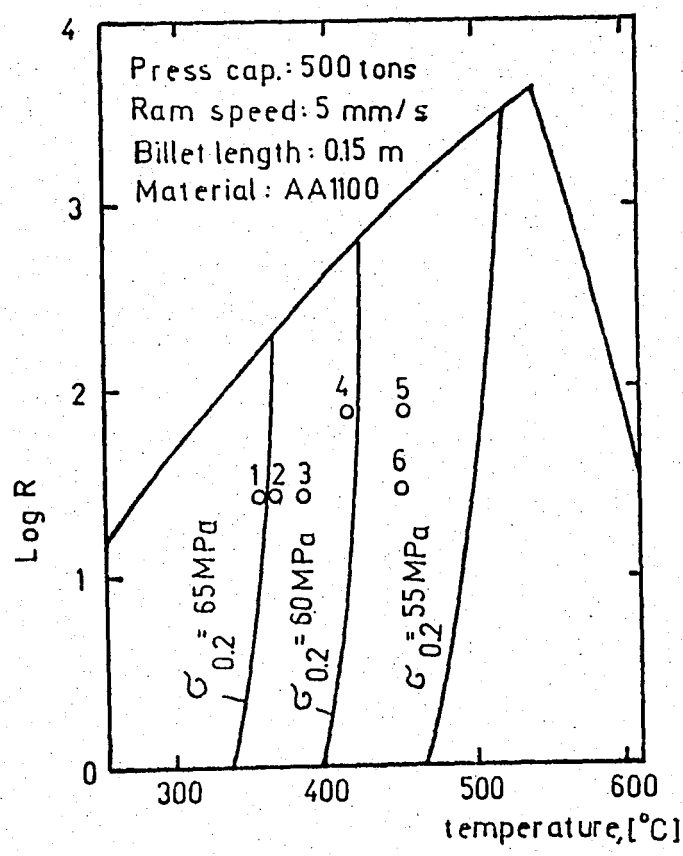

FIGURE 52. Diagram showing the proof stress values of product as a function of deformation temperature and extrusion ratio.

tests of the products agree fairly well with those shown in Fig.52 for small extrusion ratios (R=25) and low temperatures (300-400 ^{o}C), they do not for large extrusion ratios and high temperatures. This may be because of the recrystallized locations which cause the heterogeneity in the product, resulting in the decreases in the mechanical properties. So a recrystallization boundary should be added to this diagram and then it should be only used for the products which have fibrous structure. (Sheppard [29] has developed a method to draw the recrystallization boundary.)

It should be noted that the temperature values tabulated in Table 7 are the deformation temperatures. That means these temperatures are higher than the initial billet temperatures because of the temperature increase during the extrusion. Relation between the initial billet temperature, T_o and the deformation tempetature, T is:

$$T_o = T-\Delta T \qquad (36)$$

Temperature increases of the products extruded with the extrusion ratios of 25:1, 63:1 and 160:1 were calculated for steady state extrusion by means of the computer programme, and, using Eq.36, extension of the diagram given in Fig.52 to include the initial billet temperature was achieved (Fig.53). Since initial billet temperature can be easily controlled, this second diagram will be more useful in practice.

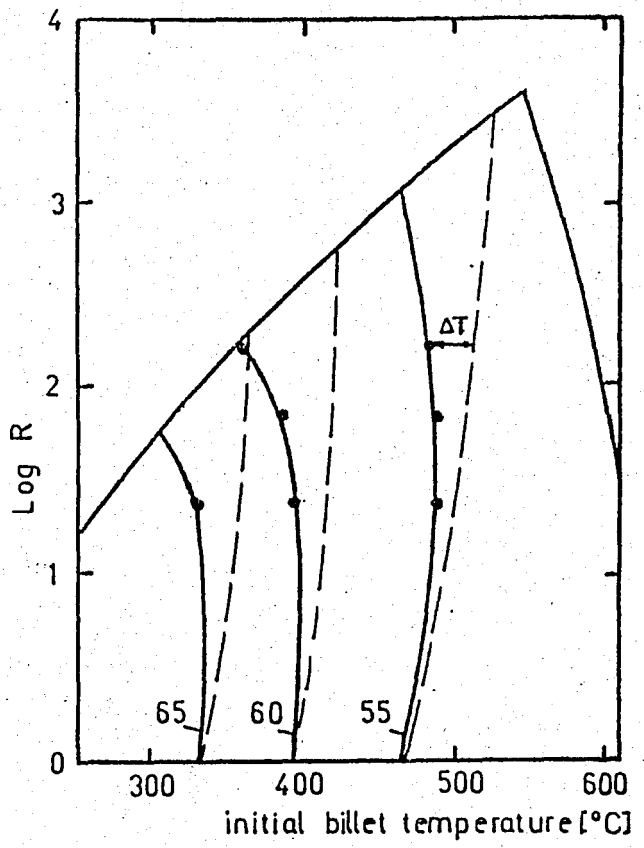

FIGURE 53. Extrusion limit diagram of AA1100, including the proof stress values of product.

Obviously, for other mechanical properties such as ultimate tensile strength, same procedure can be applied and the extrusion limit diagram can be developed so that it gives the information about those properties of product.

V. CONCLUSIONS

i) Microstructures of the extruded aluminum products are closely related to the initial billet temperature and extrusion ratio.

ii) These products may have three types of microstructures; fully recrystallized, fibrous and dublex structures.

iii) Increasing billet temperature and decreasing extrusion ratio result in increases in recrystallized grain size.

iv) Extrusion ratio effects may be recognized in the strain rate and then combined with the temperature effects in a temperature corrected strain rate term. This parameter affects the mechanical properties of the product, but it may not be only parameter operative on the properties of the product because of the precipitations in aluminum.

v) Mechanical properties of products, which have only fibrous structures, are directly related to the temperature corrected strain rate.

vi) Some parametric equations between the properties of the product and process parameters can be established. These equations can be used as limiting conditions on the limit diagram, and lead to the extrusion limit diagram as a useful tool for process control interpretation.

REFERENCES

[1] HARRIS,J.N. "Mechanical working of metals-Theory and Practise", International series on materials science technology,Volume 36, Pergamon Press, P.71-210,Oxford (1983).

[2] SHEPPARD,T.:CASTLE,A.F. "Hot working theory applied to the extrusion of some Al alloys", Metals technology, October 1986, 454-464.

[3] GEVREK,M.:ALTAN,B.:ONURLU,S. "Alüminyum ekstrüzyonunda sınır diyagram kavramı ve kullanılması", Progress Report-1, TBTAK-MAE, Gebze press(1983).

[4] GEVREK,M.:ALTAN,B.:ONURLU,S. "Ekstrüzyonda sıcaklık artışının sonlu farklar yöntemi ile bulunması", Proceedings of 1.National machine design and manufacture conference, ODTU Press,ANKARA(1984),469-476.

[5] McQUEEN,H.J. "The experimental roots of thermomechanical treatments for AL alloys", Proceedings of thermomechanical processing of AL alloys, the metallurgical society of AIME, edited by MORRIS,J.G.(1979)1-23.

[6] SHEPPARD,T. "Temperature and speed effects in hot extrusion AL alloys", Metals technology, April 1981, 130-140.

[7] SHEPPARD,T.: PATERSON,J.J. "Structural changes during thermal treatments during extrusion of AL-Cu-Mg-Mn-Si(AA 2014) alloy", Metals technology, October 1982, Vol.9, 389-398.

[8] SHEPPARD,T.:PATERSON,S.J. "Some observations of metal flow and the development of structure during the direct and indirect extrusion of commercial purity aluminum", Metals technology,October 1983, Vol.10, 361-372.

[9] McQUEEN,H.J.:JONES,J.J. "Recovery and recrystallization during high temperature deformation "Treatise on material science and technology,volume 6, Ed.by R.J.Arsenoult, Academic press, (1975),393-493.

[10] PLUMTREE,A:DEEP,G. "Microstructural misorientations in extruded aluminum", Metals technology, January 1977,1-6.

[11] BLADE,J.C. "Recrystallization in hot rolling of dilute AL alloys" Metal science, April 1979, 206-210.

[12] HASEGAWA,T.:KOCK,U.F. "Thermal recovery process in deformed aluminum", Acta metal., Vol.27, 1979, 1705-1716.

[13] SANDROM,R.:LIMDGREN,I. "The combined influence of recrystallization and recovery on stress strain curves in aluminum", Material science and engineering,47(1981),217-228.

[14] HANSEN,N.:BAY,B. "Initial stages of recrystallization in aluminum containing both large and small particles", Acta metall., 29(1981), 65-77.

[15] HANSEN,N.:BAY,B. "Initial stages of recrystallization in aluminum of commercial purity", Metall.Trans.AIME, 10A(1979),279-288.

[16] ROBINSON,D.L.:HUNTER,M.S. "Interrelation of TEM microstructure composition tensile properties and corrosion resistance of Al-Cu-Mn-Mg alloy", Metall.trans., 3(1972), 1147-1155.

[17] STYCZYNSKI,L.: PACHLA,W.: WASCIECHOWSKI,S. "Thermal softening processes in polycrystalline aluminum during hydrostatic extrusion", Metal science, 16(1982),525-528.

[18] MORRIS,P.L.:DUGGAN,B.J. "Precipitation and recrystallizatio in an AL-1.8% Mn alloy", Metal Science, January (1978),1-7

[19] SHEPPARD,T.:PARSON,N.C. "The effect of extrusion process paremeters on the microstructure and properties of an AL-Li-Mg alloy", Metal Trans., 3(1972),53-63.

[20] McQUEEN,H.J.:WONG,W.A.:JONAS,J.J. "Deformation of aluminum at high temperatures and strain rates", Canadian Journal of physics,45(1967),1225-1235.

[21] ALTAN,B.:GEVREK,M.:ONURLU,S. "Ekstrüzyon çubuklarında mikroyapı incelemeleri", Progress Report:2,TBTAK-MAE, Gebze Press (1983).

[22] SHEPPARD,D.:Raybould,D. "Axisymmetric extrusion:The effect of temperature rise and strain rate on activation enthalpy and material constants of some aluminum alloys and their relation to recrystallization,substructure and subsequent mechanical properties", J.Inst.Metals, 101(1973),65-72.

[23] GEVREK,M.:ALTAN,B.:ONURLU,S. "Ekstrüzyonda sıcaklık dağılımı için geliştirilen bir sonlu farklar modelinin incelenmesi", Progress Report:4, TBTAK-MAE,Gebze Press (1985).

[24] LATKOWSKI,A.:STEC,Z. "Effect of extrusion temperature and magnese contents on structure and properties of the ALMn SiMn alloy", Johrg., 8(1984) 606-609.

[25] ALTINTAŞ.S. "ALMgSi 0.5 ekstrüzyonu ve mekanik özelliklerine etki eden parametreler" A report of institute for graduate studies in science and engineering, B.Ü.Press, 1984.

[26] SMITH,C. "Working range of an aluminum alloy" J.Inst. Metals., 76(1950),429-435.

[27] SHEPARD,D.:PATERSON,S.J. "Direct and indirect extrusion of aluminum alloys", Met.technol., 9(1982),274-281.

[28] SHEPPARD,T. : CASTLE,A.F. "Observations on the application of limit diagrams to the aluminum alloy extrusion", Proceedings of 16.international mechine tool design and research conference, Macmillan Pres (1976),535-543.

[29] SHEPPARD,T.:RAYBOULD,D. "A new approach to the construction of extrusion limit diagrams, giving structural information with application to superpure aluminum and AL-Zn-Mg alloys", J.Inst.Metals,101(1973),73-78.

[30] ÜÇIŞIK,H. "Metalografik numune hazırlama tekniğinde dağlama ve dağlama reaktifleri" İTÜ,Faculty of metallurgy press,(1981).

APPENDICES

A - CALCULATION OF TEMPERATURE DISTRIBUTION

B - CALCULATION OF STRAIN RATE DISTRIBUTION

C - MICROSTRUCTURES OF EXTRUDED PRODUCTS

APPENDIX A

CALCULATION OF TEMPERATURE DISTRIBUTION

To calculate the temperature distribution during the extrusion process finite element method was used. A computer programme was used to determine the finite difference equations and to solve them for the nodes shown in Fig.A-1.

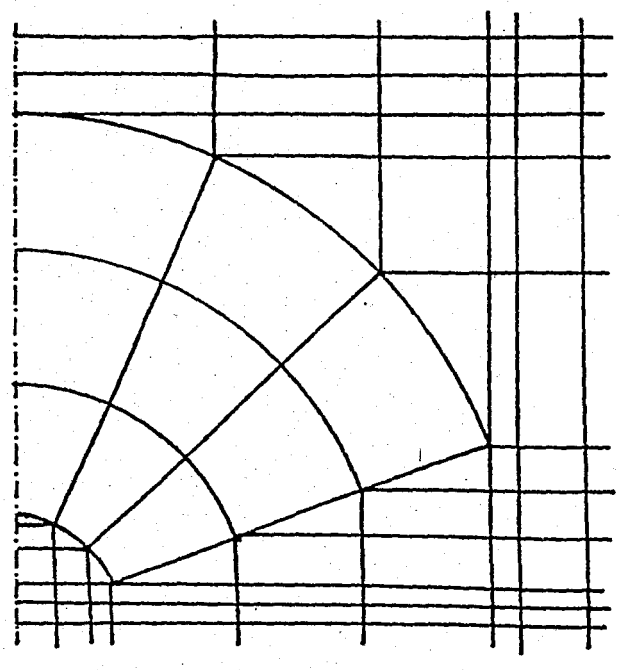

FIGURE A-1. Nodes where the temperature values were calculated.

To construct and write the programme easily, control volume was divided into six main regions; B(billet), D(deformation zone), E(product), Z(dead zone), C(container) and F(die) (Fig. A-2). All the regions were defined in cylindrical coordinates except region D which was defined in spherical coordinates. Heat conduction equations were established seperately for each region.

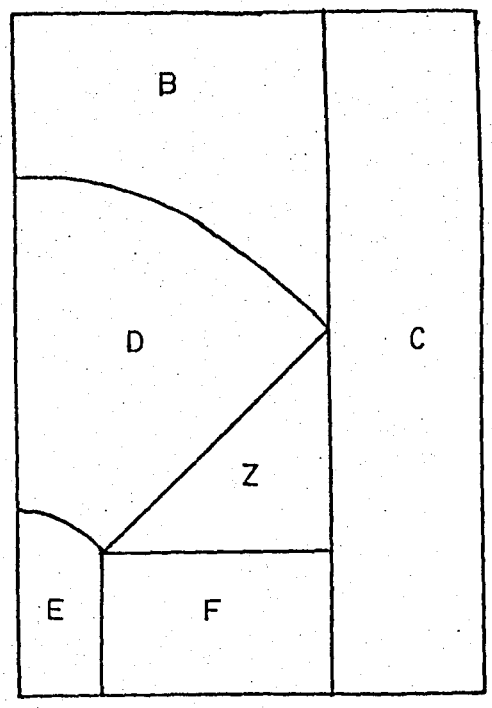

FIGURE A-2. Six main regions in the control volume.

To write the finite differences equations, it is necessary to specify the finite number of nodes in the control volume. Schematic sketch of the extrusion process used in the prog-

ramme is shown in Fig.A-3. Finite difference mesh parameters used in the computer programme are given below.

IMAX : Radial step number at Region D.

JMAX : Tangential step number at Region D.

IB : Vertical step number at Region B.

IC : Horizontal step number at Region C.

IE : Vertical step number at Region E.

IF : Vertical step number at Region F.

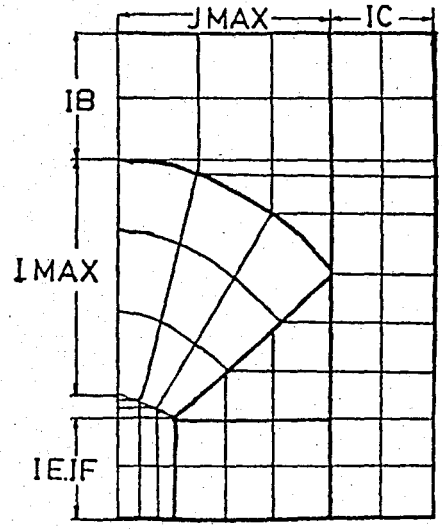

FIGURE A-3 . Finite difference mesh parameters .

The heat equations were established for each region and expressed in a linear equation

$$(\underset{\sim}{M} . \Delta t + \underset{\sim}{I}) . \vec{T} = \vec{T}' + \vec{Q} . \Delta t \qquad (A-1)$$

where $\underset{\sim}{M}$ is the heat conduction coefficient matrix, Δt is time interval, $\underset{\sim}{I}$ is unit matrix, $\vec{T}$ is temperature vector at the end of the time interval, $\vec{T}'$ is the temperature vector at the beginning of the time interval and $\vec{Q}$ is the heat generation vector.

Writing

$$\underset{\sim}{N} = \underset{\sim}{M} \cdot \Delta t + \underset{\sim}{I} \qquad \text{(A-2)}$$

and

$$\vec{P} = \vec{T}' + \vec{Q} \cdot \Delta t \qquad \text{(A-3)}$$

and substituting Eq.(A-3) and Eq.(A-2) into Eq.(A-1) yields:

$$\underset{\sim}{N} \cdot \vec{T} = \vec{P} \qquad \text{(A-4)}$$

Then we can solve $\vec{T}$, temperature vector at the end of the time interval.

Flow diagram of main computer programme which calculates the temperature distribution during the extrusion process is given in Table A-1. Parameters and subroutines used in the programme are given below.

INPUT DATA

IMAX,JMAX,IB,IC,IE,IF:Finite difference mesh parameters.

DELTAC(I) : Horizontal step dimension field at Region C.

B(I) : Vertical step coordinate field at Region B

E(I) : Vertical step coordinate field at Region E.

TABLE A-1. Flow diagram of main computer programme.

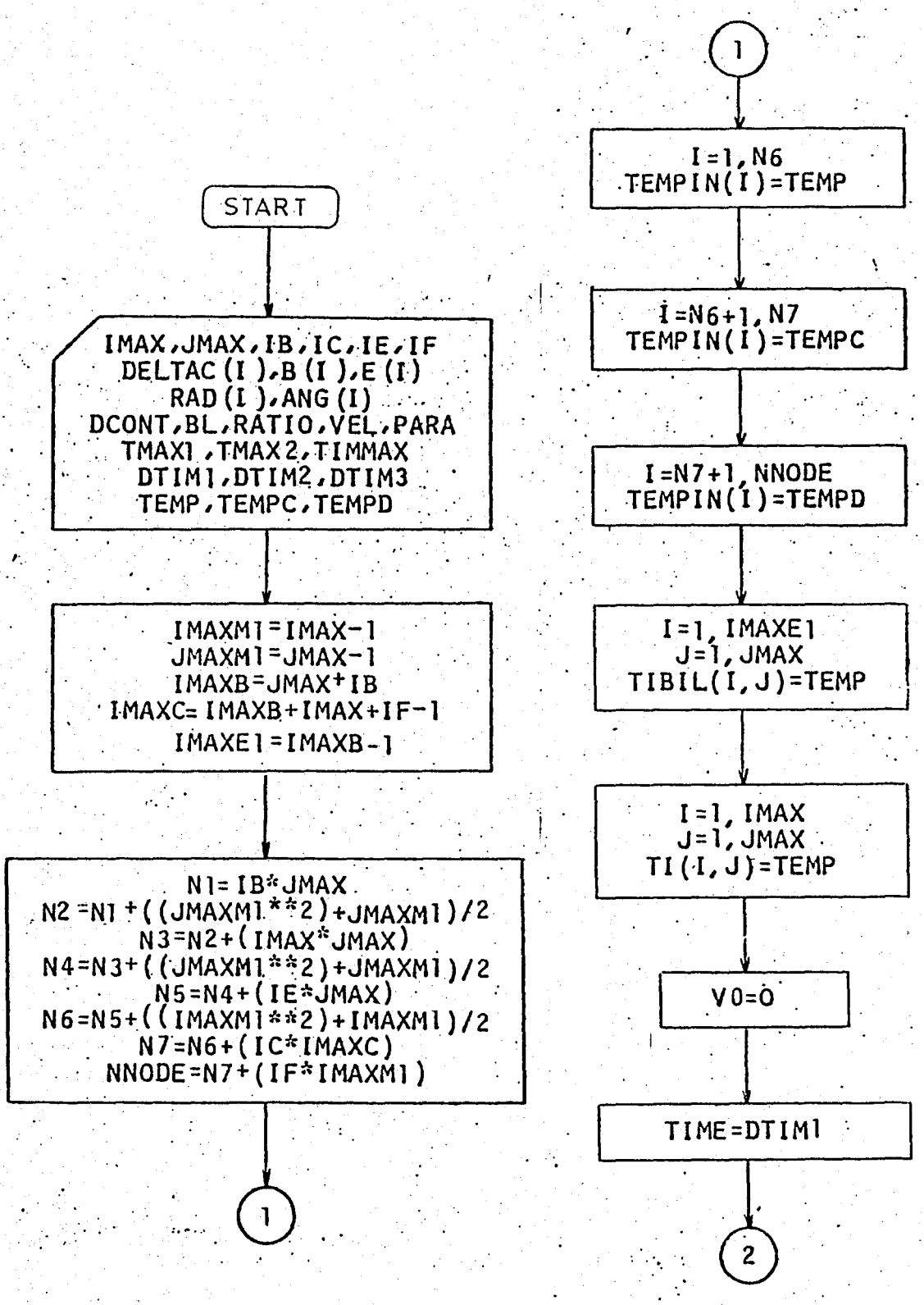

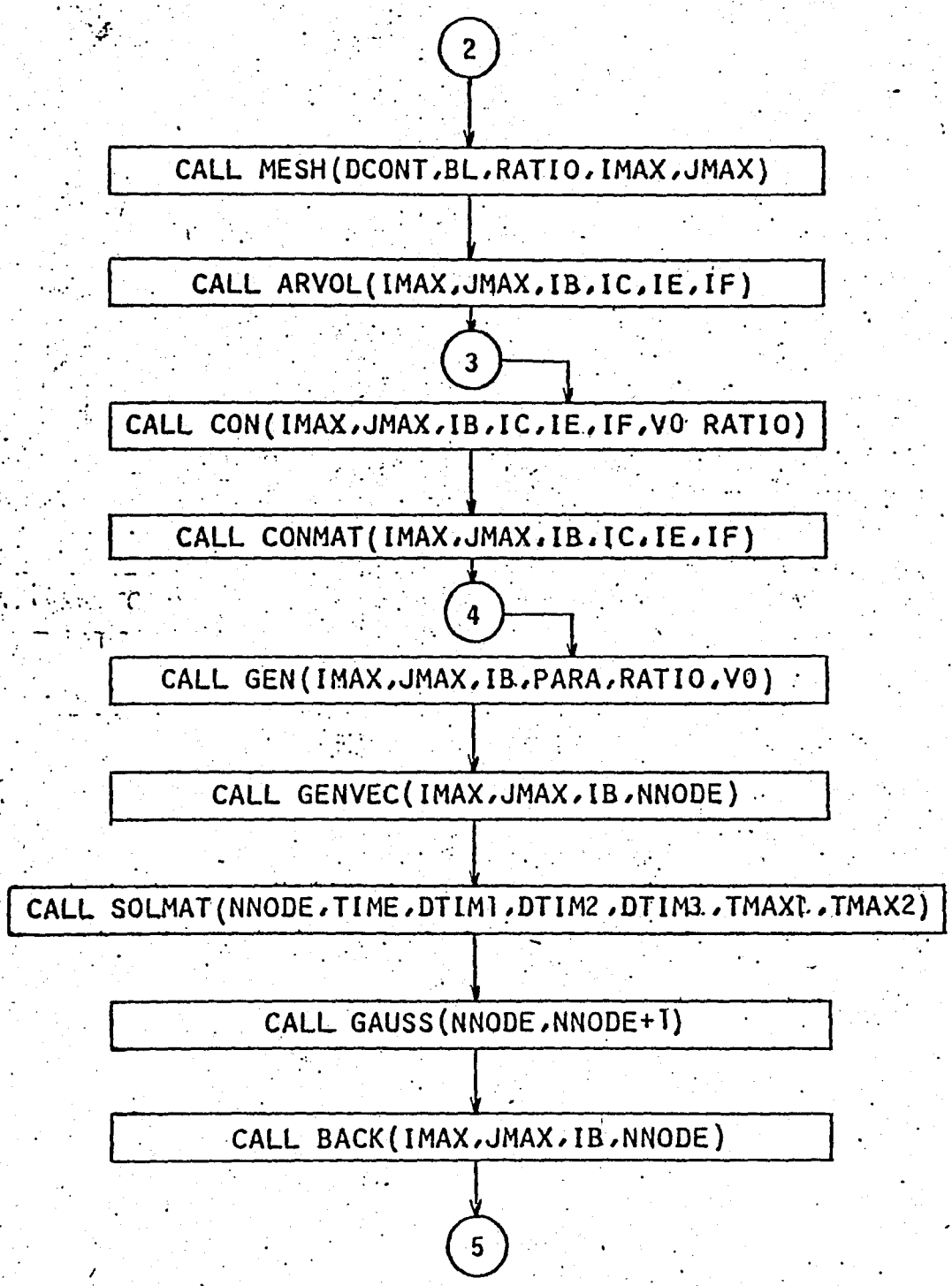
2
CALL MESH(DCONT,BL,RATIO,IMAX,JMAX)
CALL ARVOL(IMAX,JMAX,IB,IC,IE,IF)
3
CALL CON(IMAX,JMAX,IB,IC,IE,IF,V0 RATIO)
CALL CONMAT(IMAX,JMAX,IB,IC,IE,IF)
4
CALL GEN(IMAX,JMAX,IB,PARA,RATIO,V0)
CALL GENVEC(IMAX,JMAX,IB,NNODE)
CALL SOLMAT(NNODE,TIME,DTIM1,DTIM2,DTIM3,TMAX1,TMAX2)
CALL GAUSS(NNODE,NNODE+1)
CALL BACK(IMAX,JMAX,IB,NNODE)
5

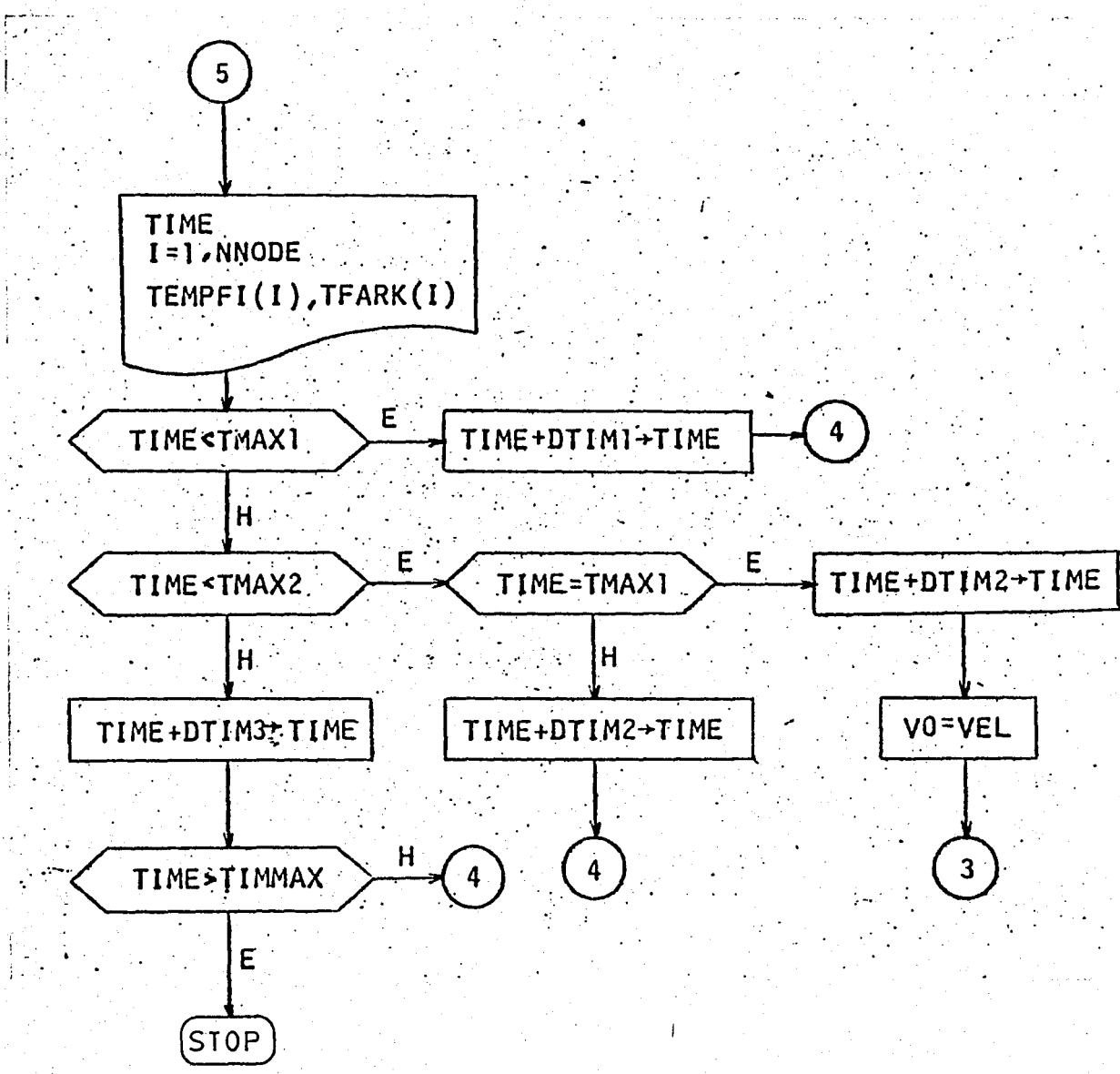
5
TIME
I=1,NNODE
TEMPFI(I),TFARK(I)
TIME<TMAX1
E
TIME+DTIM1→TIME
4
H
TIME<TMAX2
E
TIME=TMAX1
E
TIME+DTIM2→TIME
H
H
TIME+DTIM3→TIME
TIME+DTIM2→TIME
VO=VEL
TIME>TIMMAX
H
4
4
3
E
STOP

RAD(I) : Radial step factor field at Region D.

ANG(I) : Tangential step factor field at Region D.

DCONT : Container diameter.

BL : Billet Length.

RATIO : Extrusion ratio.

VEL : Extrusion velocity.

PARA : Strain rate parameter.

TIMMAX : Total time.

DTIM : Time interval.

TEMP : Initial billet temperature.

TEMPC : Initial container temperature.

TEMPD : Initial die temperature.

VARIABLES

VØ : Extrusion velocity.

TIME : Time

TIBIL(I) : Temperature field at region B.

T.I(I,J) : Temperature field at region D.

TEMPIN(I) : Initial temperature field.

TEMPFI(I) : Calculated temperature field.

TFARK(I) : Calculated temperature rise field.

SUBROUTINES

MESH : Calculates the coordinates of the nodes and elements defined around the nodes.

ARVOL : Calculates the volumes and the surface areas of the volume elements around the nodes.

CON : Calculates heat transfer equation coefficients for the nodes at each region.

CONMAT : Collects the heat transfer equation coefficients calculated by CON in a matrix.

GEN : Calculated the heat generation values at deformation zone.

GENVEC : Collects the heat generation values in a general hea generation vector.

GAUSS : Solves the expanded solution matrix by gauss elimination method and calculates the temperatures at the nodes.

SOLMAT : Determines the expanded solution matrix.

BACK : Set the calculated temperatures as initial temperatures for the next time step.

List of main programme to calculate the temperature distribution during extrusion is given in Table A-2.

Outputs of this program for R = 25 at T_o = 350^{o}C and R = 63 at T_o = 400 ^{o}C are given in Table A-3 and Table A-4 respectively.

TABLE A-2.List of main programme.

```
C*************************************************************
C*      MAIN PROGRAMME TO CALCULARE THE TEMPERATURE DISTRIBUTION
C*     DURING THE EXTRUSION
C*************************************************************

      COMMON/XXX/DI(10),DJ(10),DJD(10),DAI(11),DAJ(11),
     1BI(15),BJ(10),BAI(16),BAJ(11),EI(15),EJ(10),EAI(16),EAJ(11),
     1ZI(10),ZJ(10),ZAI(11),ZAJ(11),CI(30),CJ(5),CAI(30),CAJ(5),
     1FI(5),FJ(10),FAI(5),FAJ(10),
     1TOPAD(10,10),BOTAD(10,10),SIDAD(10,10),VOLD(10,10),
     1TOPAB(15,10),BOTAB(15,10),SIDAB(15,10),VOLB(15,10),
     1TOPAE(15,10),BOTAE(15,10),SIDAE(15,10),VOLE(15,10),
     1TOPAZ(10,10),BOTAZ(10,10),SIDAZ(10,10),VOLZ(10,10),
     1TOPAC(30,5),BOTAC(30,5),SIDAC(30,5),VOLC(30,5),
     1TOPAF(5,10),BOTAF(5,10),SIDAF(5,10),VOLF(5,10),
     1VOLDB(10,10),VOLBB(15,10),VOLEB(15,10),VOLZB(10,10),VOLFB(5,10)
     1AREAD(10,10),AREAB(15,10),AREAE(15,10),B(6),E(6),DELTAC(5)
      COMMON/XXY/DK(50,50),BK(70,70),EK(70,70),
     1ZK(65,65),CK(80,80),FK(35,35)
      COMMON/XXZ/GK(205,205)
      COMMON/YYX/TIBIL(15,10),TI(10,10),TIAES(10,10)
      COMMON/YYY/ZEBIL(15,10),SIGBIL(15,10),STRATE(10,10),ZENER(10,10
     1SIGMA(10,10),TETACR(10)
      COMMON/YYZ/SK(100),DSK(100)
      COMMON/ZZX/VSK(205)
      COMMON/ZZY/TEMPIN(205),TEMPFI(205)
      COMMON/ZZZ/VSKP(205),GKP(205,205),GKPAUG(205,205)
      COMMON/FFF/TFARK(205)
      COMMON/MMM/RAD(10),ANG(10)
      COMMON/PPP/TINC(205)
      COMMON/TTT/TFINC(205)

C*************************************************************
C*          FINITE DIFFERENCE MESH PARAMETERS
C*************************************************************
C*     IMAX,JMAX:VERTICAL AND HORIZENTAL MESH LINES AT DEF. ZONE
C*     IB        :VERTICAL STEPSAT THE TOP OF BILLET
C*     IC        :HORIZENTAL STEPS AT CONTAINER
C*     ID        :VERTICAL STEPS AT THE BOTTON OF PRODUCT
C*     IF        :VERTICAL STEPS AT DIE
C*************************************************************

C*************************************************************
C         INPUT DATA
C*************************************************************
      WRITE(5,509)
509   FORMAT(//'*************************************************
     1*******'/'THIS PROGRAMME CALCULATES TEMPERATURE DISTRIBUTION I
     1TRUSION'/'*************************************************
     1*******'///)
      WRITE(5,510)
510   FORMAT('ENTER IMAX,JMAX,IB,IC,IE,IF (FORMAT:6I1) :')
      READ(5,5102)IMAX,JMAX,IB,IC,IE,IF
```

```
5102 FORMAT(8F1)
     IMAXM2=IMAX-2
     JMAXM2=JMAX-2
     READ(4,512)(DELTAC(K),K=1,IC)
     READ(4,513)(B(K),K=1,IB)
     READ(4,514)(E(K),K=1,IE)
     WRITE(5,521)
 521 FORMAT('ENTER CONTAINER DIAMETER(M) :')
     READ(5,*)DCONT
     WRITE(5,522)
 522 FORMAT('ENTER BILLET LENGTH(M) :')
     READ(5,*)BL
     WRITE(5,523)
 523 FORMAT('ENTER RADIUS DIVISION FACTORS (IMAX-2) :')
     READ(5,*)(RAD(I),I=1,IMAXM2)
     WRITE(5,524)
 524 FORMAT('ENTER ANGLE DIVISION FACTORS (JMAX-2) :')
     READ(5,*)(ANG(J),J=1,JMAXM2)
     WRITE(5,525)
 525 FORMAT('ENTER EXTRUSION RATIO :')
     READ(5,*)RATIO
     WRITE(5,526)
 526 FORMAT('ENTER INTERMEDIATE TIMES T1,T2 & MAXIMUM TIME (SEC) :'
     READ(5,*)TMAX1,TMAX2,TIMMAX
     WRITE(5,527)
 527 FORMAT('ENTER TIME INCREMENTS DELTAT1,DELTAT2,DELTAT3 (SEC) :'
     READ(5,*)DTIM1,DTIM2,DTIM3
     WRITE(5,528)
 528 FORMAT('ENTER INITIAL TEMPERATURES OF BILLET,CONTAINER & DIE :
     READ(5,*)TEMP,TEMPC,TEMPD
     WRITE(5,529)
 529 FORMAT('ENTER EXTRUSION SPEED (M/SEC) :')
     READ(5,*)VEL
     WRITE(5,530)
 530 FORMAT('ENTER CONSTANT U :')
     READ(5,*)U
     WRITE(5,531)
 531 FORMAT('ENTER NO OF THE NODE TO BE PRINTED(MAX 4 PTS.)')
     READ(5,*)ND1,ND2,ND3,ND4
     WRITE(5,532)
 532 FORMAT('ENTER BILLET-CONTAINER INTERFACE STRAIN-RATE PARAMETER
     READ(5,*)PARA


     V0=0.0
     TIME=DTIM1
     EPS=0.0001

     IMAXM1=IMAX-1
     JMAXM1=JMAX-1
     IMAXB=JMAX+IB
     IMAXC=IMAXB+IMAX+IF-1
     N1=IB*JMAX
     N2=N1+((JMAXM1**2)+JMAXM1)/2
     N3=N2+IMAX*JMAX
```

```
      N4=N3+((JMAXM1**2)+JMAXM1)/2
      N5=N4+IE*JMAX
      N6=N5+((IMAXM1**2)+IMAXM1)/2
      N7=N6+IC*IMAXC
      NNODE=N7+IF*IMAXM1
      NNODE1=NNODE+1
      N=NNODE
      NP1=N+1

      ***************************************************
       SETTING BILLET,CONTAINER AND DIE TEMPERATURES
      ***************************************************
      TABS=TEMP+273.
      TABSC=TEMPC+273.
      TABSD=TEMPD+273.
      DO 1000 I=1,NNODE
      IF(I.GT.No) GO TO 1010
      TEMPFI(I)=TABS
      GO TO 1000
1010  IF(I.GT.N7) GO TO 1020
      TEMPFI(I)=TABSC
      GO TO 1000
1020  TEMPFI(I)=TABSD
1000  CONTINUE
      ***************************************************
         SETTING BILLET DIE SURFACE TEMPERATURES
      ***************************************************
      TEMPFI(N2+JMAX)=(TABS+TABSD)/2.
      DO 1001 I=1,IMAXM1
      TEMPFI(N5+I)=(TABS+TABSD)/2.
1001  CONTINUE
      DO 1002 I=1,IE
      TEMPFI(N4+(I*JMAX))=(TABS+TABSD)/2.
1002  CONTINUE
      ***************************************************
      DO 995 I=1,NNODE
      TINC(I)=TEMPFI(I)-273.
 995  CONTINUE
      IMAXE1=IMAXB-1
      DO 1200 I=1,IMAXE1
      DO 1200 J=1,JMAX
      TIBIL(I,J)=TABS
1200  CONTINUE
      DO 900 I=1,IMAX
      DO 900 J=1,JMAX
      TI(I,J)=TEMP
 900  CONTINUE
      DO 990 I=1,NNODE
      TEMK(I)=0.
 990  CONTINUE

            OUTPUT FORMATS
      WRITE(7,2029)
      WRITE(7,2030) RATIO,DCONT,BL,VEL,TEMP,TEMPC,TEMPD
      WRITE(7,981) ND1,ND2,ND3,ND4
```

```
981   FORMAT(///22X,'DUGUM NOKTALARININ SICAKLIKLARI'/3X,'ZAMAN(SN)',
     1,I2,8X,I2,8X,I2,8X,I2/3X,'**********',3X,'**********
     2**********')
      WRITE(6,2031)
      WRITE(6,2032)
      WRITE(6,2033)(I,TINC(I),I=1,NNODE)


      ***********************************************************
                        SUBROUTINES
      ***********************************************************
      CALL MESH(DCONT,BL,RATIO,IMAX,JMAX)
      CALL ARVOL(IMAX,JMAX,IB,IC,IE,IF)
1500  CALL CONI(IMAX,JMAX,IB,IC,IE,IF,VO,RATIO,U,TIME,TMAX1,EPS)
      CALL CONMAT(IMAX,JMAX,IB,IC,IE,IF)
1600  CALL GEN(IMAX,JMAX,IB,PARA,RATIO,VO)
      CALL GENVEC(IMAX,JMAX,IB,NNODE)
      CALL SOLMAT(NNODE,TIME,DTIM1,DTIM2,DTIM3,TMAX1,TMAX2)
      CALL GAUSS(N,NP1)
      CALL BACK(IMAX,JMAX,IB,NNODE)

        OUTPUT TERMS
      WRITE(5,2110)TIME
2110  FORMAT('TIME=',F25.20)
      WRITE(5,1110)VO
1110  FORMAT('VO=',F9.5)
      WRITE(7,4098)
      WRITE(6,2000)TIME
      WRITE(6,2010)
      WRITE(6,617)(I,TFINC(I),I=1,NNODE)
      WRITE(6,3000)TIME
      WRITE(6,3010)
      WRITE(6,717)(I,TFARK(I),I=1,NNODE)
      WRITE(7,982)TIME,TFINC(ND1),TFINC(ND2),TFINC(ND3),TFINC(ND4)
982   FORMAT(F11.4,5X,4F10.2)

        TIME INTERVAL
      IF(TIME.GE.TMAX1)GO TO 2
      TIME=TIME+DTIM1
      GO TO 1600
    2 VO=VEL
      IF(TIME.GE.TMAX2-EPS)GO TO 4
      IF(TIME.EQ.TMAX1) GO TO 3
      TIME=TIME+DTIM2
      GO TO 1600
    3 TIME=TIME+DTIM2
      GO TO 1500
    4 TIME=TIME+DTIM3
      IF(TIME.LE.TIMMAX-EPS) GO TO 1600
      STOP

        INPUT FORMATS
  512 FORMAT(6F5.3)
  513 FORMAT(6F5.3)
  514 FORMAT(F6.4,5F5.3)
```

```
      OUTPUT FORMATS
2029 FORMAT(//4X,'*************************************************
     1*************'/4X,'*  ,TEMPERATURE DISTRIBUTION DURING EXTRU
     1     SION PROCESS          *'/4X,'*************************
     1*************************'///)
2030 FORMAT(/8X,'  EXTRUSION RATIO = ',F5.1,/8X,'BILLET DIAMETER  = '
     1F5.3,'  M',/8X ,'BILLET LENGTH     = ',F5.3,'  M',/8X,'PRESS VEL
     1     = ',F5.3,'  M/SN',/8X,'BILLET TEMPERATURE ',F5.1,'  C',/8X
     1'CONTAINER TEMP.  = ',F5.1,'  C',/8X,'DIE TEMPERATURE  = ',F5.1
     1'  C')
2031 FORMAT(////10X,'INITIAL TEMPERATURE DISTRIBUTION (C)')
2032 FORMAT(10X,'**************************************'/)
2033 FORMAT(10('(',I3,')',F6.1,2X))
4098 FORMAT(//)
2000 FORMAT(//10X,F5.2,1X,'SECOND AFTER, TEMPERATURE DISTRIBUTION (C
2010 FORMAT(10X,'**************************************************'/)
 617 FORMAT(10('(',I3,')',F6.1,2X))
3000 FORMAT(//10X,F5.2,1X,' SECOND AFTER, TEMPERATURE RISES')
3010 FORMAT(10X,'**************************************************'/)
 717 FORMAT(10('(',I3,')',F6.1,2X))
     END
```

TABLE A-3. Output of the main programme for R=25 and T_o=350°C .

TEMPERATURE DISTRIBUTION DURING EXTRUSION PROCESS

EXTRUSION RATIO	= 25.0	
BILLET DIAMETER	= 0.100	M
BILLET LENGTH	= 0.150	M
PRESS VELOCITY	= 0.005	M/SN
BILLET TEMPERATURE	= 350.0	C
CONTAINER TEMP.	= 263.0	C
DIE TEMPERATURE	= 202.0	C

	(TEMPERATURES AT NODES			
TIME (SN)	31	32	33	34
2.0000	347.72	347.63	347.52	347.60
4.0000	344.12	344.01	343.83	344.01
6.0000	339.85	339.75	339.54	339.80
8.0000	335.44	335.35	335.13	335.43
10.0000	331.21	331.13	330.91	331.21
10.5000	336.65	335.73	335.69	334.71
11.0000	343.79	342.94	342.91	341.87
11.5000	347.38	346.87	346.78	346.17
12.0000	349.54	349.23	349.14	348.80
12.5000	351.08	350.88	350.81	350.60
13.0000	352.27	352.14	352.12	351.97
13.5000	353.27	353.20	353.21	353.10
14.0000	354.15	354.11	354.17	354.07
14.5000	355.48	355.47	355.61	355.45
15.0000	356.90	356.92	357.15	356.94
18.0000	361.69	361.39	362.55	362.11
21.0000	362.93	363.23	364.06	363.54
24.0000	363.92	364.20	365.22	364.63
27.0000	364.84	365.22	366.26	365.62

TABLE A-4. Output of main programme for R=63 and T_o = 400 ^oC.

TEMPERATURE DISTRIBUTION DURING EXTRUSION PROCESS

EXTRUSION RATIO	= 63.0	
BILLET DIAMETER	= 0.100	M
BILLET LENGTH	= 0.150	M
PRESS VELOCITY	= 0.005	M/SN
BILLET TEMPERATURE	= 400.0	C
CONTAINER TEMP.	= 350.0	C
DIE TEMPERATURE	= 300.0	C

	TEMPERATURES AT NODES			
TIME (SN)	31	32	33	34
2.0000	398.26	398.20	398.16	398.18
4.0000	395.92	395.85	395.79	395.85
6.0000	393.29	393.23	393.16	393.25
8.0000	390.63	390.58	390.50	390.62
10.0000	388.11	388.06	387.99	388.11
10.5000	399.51	398.78	398.72	397.77
11.0000	409.77	409.41	409.38	408.87
11.5000	413.70	413.58	413.61	413.38
12.0000	415.96	415.90	416.05	415.90
12.5000	417.65	417.67	417.81	417.69
13.0000	418.99	419.04	419.23	419.09
13.5000	420.13	420.20	420.44	420.28
14.0000	421.13	421.22	421.50	421.33
14.5000	422.65	422.75	423.13	422.87
15.0000	424.19	424.30	424.77	424.44
18.0000	429.01	429.21	430.06	429.42
21.0000	430.08	430.31	431.27	430.56
24.0000	431.01	431.26	432.31	431.53
27.0000	431.82	432.09	433.19	432.38

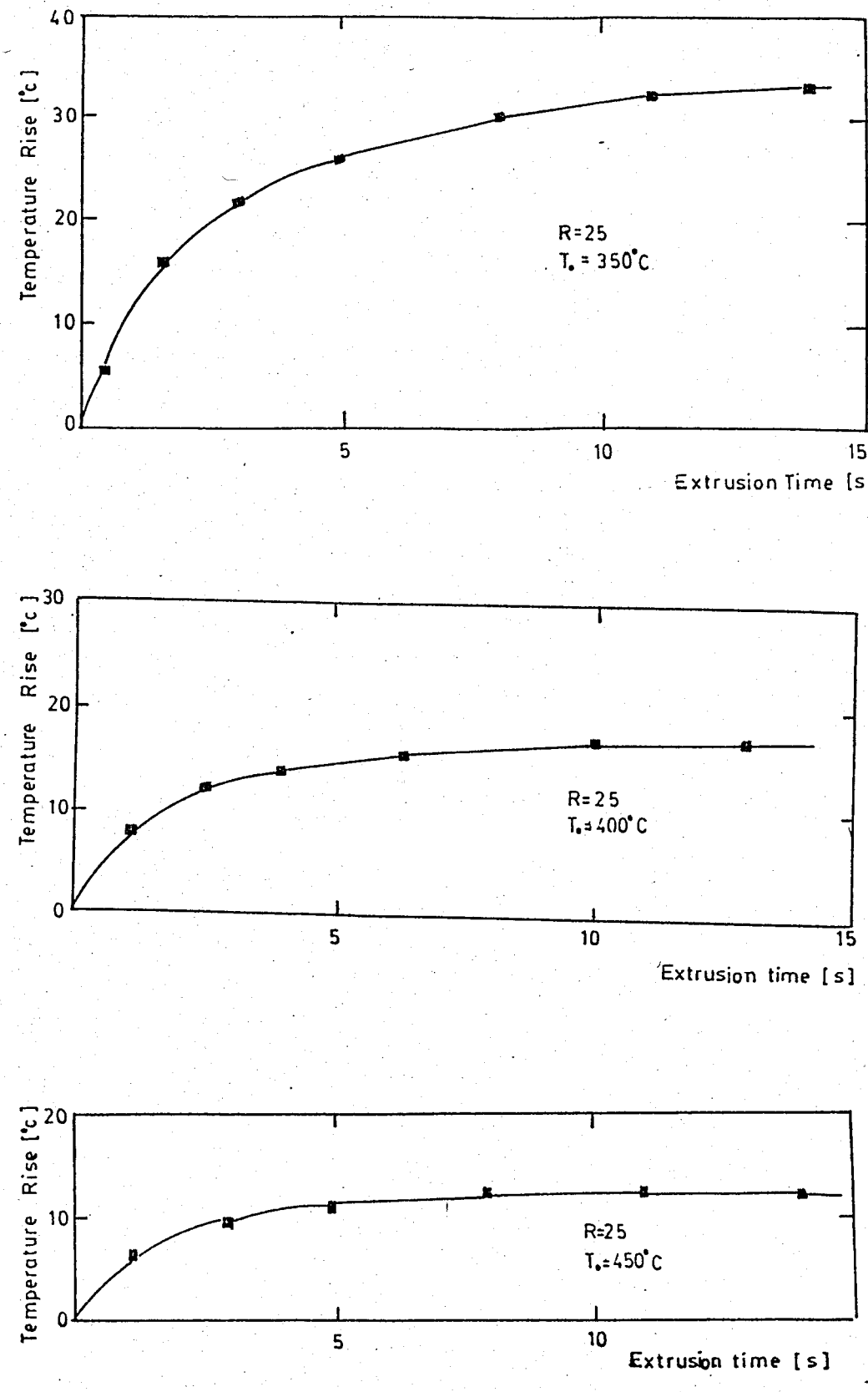

FIGURE A-4. Temperature rise calculated by finite difference computer programme for R=25 at varying initial billet temperatures.

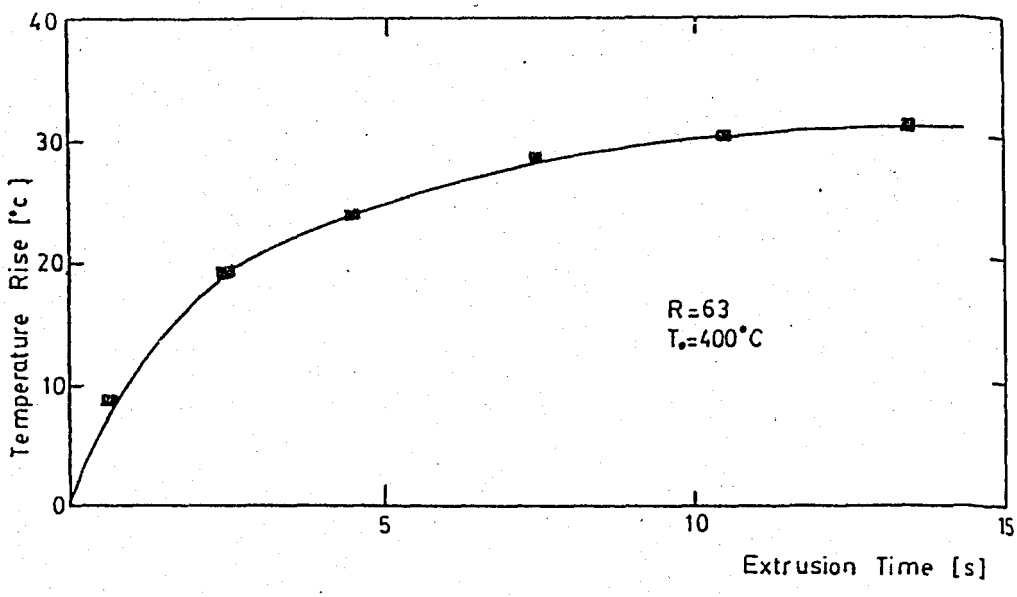

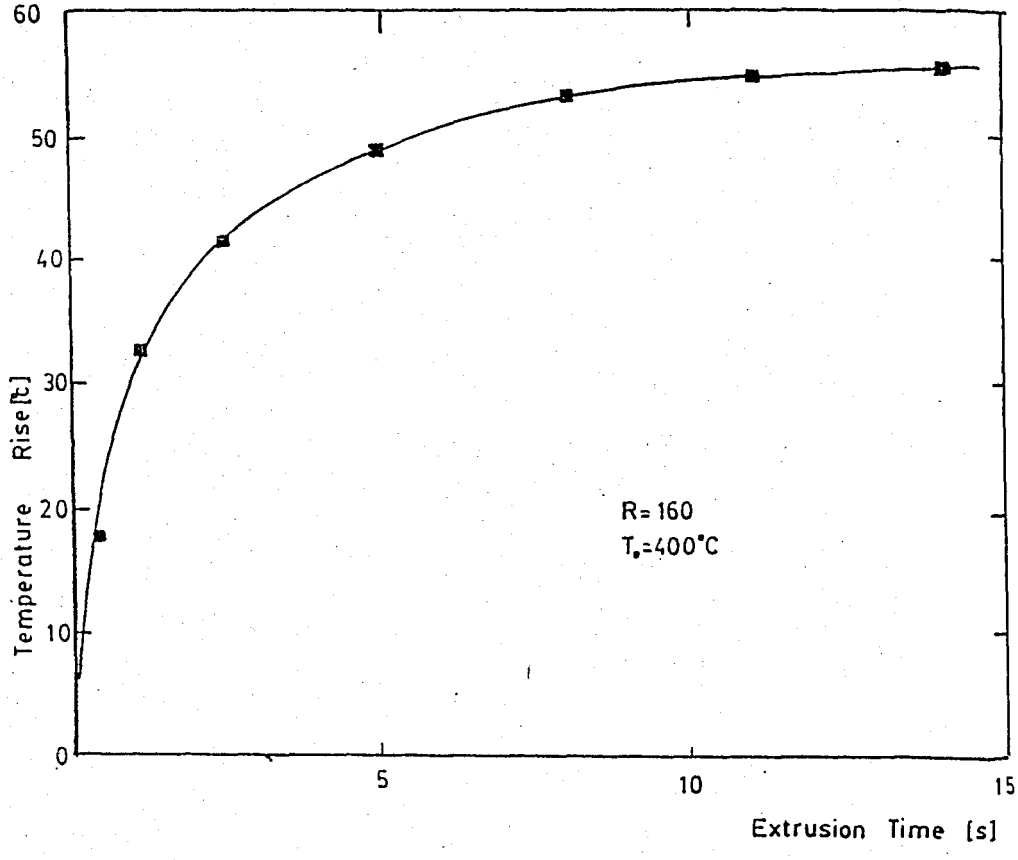

FIGURE A-5. Temperature rise calculated by finite difference computer programme for varying extrusion ratios at 400°C initial billet temperature..

Temperature rise during extrusion process calculeted by this computer programme is plotted against the extrusion time. Fig.A-4 shows the temperature rise for the extrusion ratio of 25:1 at 350^{o}C, 400^{o}C and 450^{o}C initial billet temperatures. It can be seen that increasing initial billet temperature causes a decrease in the temperature rise during extrusion.

Fig.A-5 shows the temperature rise for the extrusion ratios of 63:1 and 160:1 at 400^{o}C initial billet temperature. It can be seen that increasing initial billet temperature results in an increase in temperature rise.

APPENDIX B

CALCULATION OF STRAIN RATE DISTRIBUTION

For the analyses of deformation during the direct extrusion process, spherical velocity field model, first suggested by Avitzur [21], was used. According to this model, material moves during the extrusion process as shown in Fig.B-1.

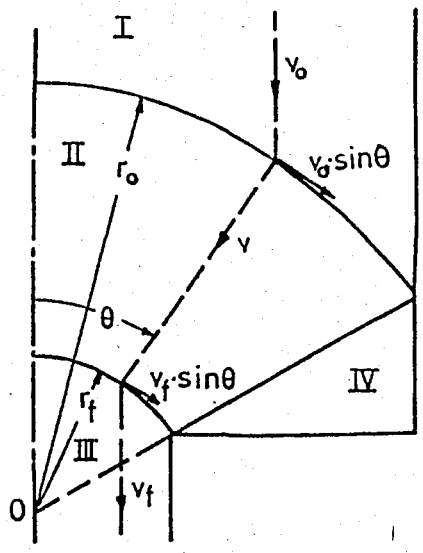

FIGURE B-1. Avitzur's spherical velocity field model.

At region I, namely the billet, material flows with a uniform velocity, V_o, parallel to the centerline. At Region I namely the deformation zone, material moves on the lines, which pass through a point on the centerline with a velocity

$$V = - V_o r_o^2 \frac{\cos\theta}{r^2} \tag{B-1}$$

where r is the distance between any point in the deformation zone and point 0, and θ is the angle between the line that connects that point to point 0, and the centerline.

For deformation zone, the velocity components in spheric coordinates can be written as [21]

$$V_r = V = - V_o R_o^2 \frac{\cos\theta}{R^2} \tag{B-2}$$

$$V_\theta = 0 \tag{B-3}$$

$$V_\phi = 0 \tag{B-4}$$

Region III, or product has a uniform velocity, V_f, parallel to the centerline. In Region IV, namely the dead zone materi does not move.

Using Eq.s(B-2)-(B-4), strain rates can be calculated in spherical coordinates as [21]

$$\dot{\varepsilon}_{rr} = - 2\dot{\varepsilon}_{\theta\theta} = - 2 \dot{\varepsilon}_{\phi\phi} = 2V_f r_f \frac{\cos\theta}{r^3} \tag{B-5}$$

$$\dot{\varepsilon}_{r\theta} = \frac{1}{2} V_f r_f^2 \frac{\sin\theta}{r^3} \tag{B-6}$$

$$\dot{\varepsilon}_{\phi\theta} = \varepsilon_{r\phi} = 0 \qquad \text{(B-7)}$$

A computer programme was developed in the light of information given above so that the strain rate values in the deformation zone could be determined.

Results of the programme are denoted by the followings

REX(MM) : Distances from the Point 0(r)

TEXT(RAD):Angles to the centerline (θ)

SR(1/SN): Strain rates

Outputs of this programme for R = 25 and R = 63 are given in Table B-1 and Table B-2 respectively.

TABLE B-1. Output of the Computer programme which calculates the strain rate distribution, for R=25.

STRAIN RATE DISTRIBUTION

EXTRUSION RATIO:25

REX(MM)	TEXT(RAD)	SR(1/SN)	REX(MM)	TEXT(RAD)	SR(1/SN)
11.015	0.00000	4.53707	11.015	0.34141	4.29953
13.219	0.00000	2.62678	13.219	0.34141	2.48815
15.422	0.00000	1.65418	15.422	0.34141	1.56688
17.625	0.00000	1.10817	17.625	0.34141	1.04969
19.828	0.00000	0.77831	19.828	0.34141	0.73723
22.031	0.00000	0.56738	22.031	0.34141	0.53744
24.234	0.00000	0.42628	24.234	0.34141	0.40379
26.437	0.00000	0.32835	26.437	0.34141	0.31102
28.640	0.00000	0.25825	28.640	0.34141	0.24463
30.843	0.00000	0.20677	30.843	0.34141	0.19586
33.046	0.00000	0.16811	33.046	0.34141	0.15924
35.249	0.00000	0.13852	35.249	0.34141	0.13121
37.453	0.00000	0.11549	37.453	0.34141	0.10939
39.656	0.00000	0.09729	39.656	0.34141	0.09215
41.859	0.00000	0.08272	41.859	0.34141	0.07836
44.062	0.00000	0.07092	44.062	0.34141	0.06718
46.265	0.00000	0.06127	46.265	0.34141	0.05803
48.468	0.00000	0.05329	48.468	0.34141	0.05047
50.671	0.00000	0.04663	50.671	0.34141	0.04417
52.874	0.00000	0.04104	52.874	0.34141	0.03888
55.077	0.00000	0.03631	55.077	0.34141	0.03440

REX(MM)	TEXT(RAD)	SR(1/SN)	REX(MM)	TEXT(RAD)	SR(1/SN)
11.015	0.17071	4.47863	11.015	0.51212	4.00850
13.219	0.17071	2.59180	13.219	0.51212	2.31974
15.422	0.17071	1.63215	15.422	0.51212	1.46082
17.625	0.17071	1.09342	17.625	0.51212	0.97864
19.828	0.17071	0.76794	19.828	0.51212	0.68733
22.031	0.17071	0.55983	22.031	0.51212	0.50106
24.234	0.17071	0.42061	24.234	0.51212	0.37646
26.437	0.17071	0.32398	26.437	0.51212	0.28997
28.640	0.17071	0.25482	28.640	0.51212	0.22807
30.843	0.17071	0.20402	30.843	0.51212	0.18260
33.046	0.17071	0.16588	33.046	0.51212	0.14846
35.249	0.17071	0.13668	35.249	0.51212	0.12233
37.453	0.17071	0.11395	37.453	0.51212	0.10197
39.656	0.17071	0.09599	39.656	0.51212	0.08592
41.859	0.17071	0.08162	41.859	0.51212	0.07305
44.062	0.17071	0.06998	44.062	0.51212	0.06263
46.265	0.17071	0.06045	46.265	0.51212	0.05410
48.468	0.17071	0.05258	48.468	0.51212	0.04706
50.671	0.17071	0.04601	50.671	0.51212	0.04118
52.874	0.17071	0.04050	52.874	0.51212	0.03625
55.077	0.17071	0.03583	55.077	0.51212	0.03207

REX(MM)	TEXT(RAD)	SR(1/SN)	REX(MM)	TEXT(RAD)	SR(1/SN)
11.015	0.68283	3.61714	11.015	1.02424	2.41150
13.219	0.68283	2.09325	13.219	1.02424	1.51117
15.422	0.68283	1.31520	15.422	1.02424	0.95164
17.625	0.68283	0.88309	17.625	1.02424	0.63752
19.828	0.68283	0.62022	19.828	1.02424	0.44775
22.031	0.68283	0.45214	22.031	1.02424	0.32641
24.234	0.68283	0.33970	24.234	1.02424	0.24524
26.437	0.68283	0.26166	26.437	1.02424	0.18890
28.640	0.68283	0.20580	28.640	1.02424	0.14857
30.843	0.68283	0.16478	30.843	1.02424	0.11896
33.046	0.68283	0.13397	33.046	1.02424	0.09671
35.249	0.68283	0.11039	35.249	1.02424	0.07969
37.453	0.68283	0.09203	37.453	1.02424	0.06644
39.656	0.68283	0.07753	39.656	1.02424	0.05597
41.859	0.68283	0.06592	41.859	1.02424	0.04759
44.062	0.68283	0.05652	44.062	1.02424	0.04080
46.265	0.68283	0.04882	46.265	1.02424	0.03525
48.468	0.68283	0.04246	48.468	1.02424	0.03065
50.671	0.68283	0.03716	50.671	1.02424	0.02683
52.874	0.68283	0.03271	52.874	1.02424	0.02361
55.077	0.68283	0.02894	55.077	1.02424	0.02089

REX(MM)	TEXT(RAD)	SR(1/SN)
11.015	0.85353	3.14281
13.219	0.85353	1.81875
15.422	0.85353	1.14534
17.625	0.85353	0.76729
19.828	0.85353	0.53889
22.031	0.85353	0.39285
24.234	0.85353	0.29515
26.437	0.85353	0.22734
28.640	0.85353	0.17881
30.843	0.85353	0.14317
33.046	0.85353	0.11640
35.249	0.85353	0.09591
37.453	0.85353	0.07996
39.656	0.85353	0.06736
41.859	0.85353	0.05728
44.062	0.85353	0.04911
46.265	0.85353	0.04242
48.468	0.85353	0.03689
50.671	0.85353	0.03229
52.874	0.85353	0.02842
55.077	0.85353	0.02514

TABLE B-2. Output of the computer programme which calculates the strain rate distribution, for R=63 .

STRAIN RATE DISTRIBUTION

EXTRUSION RATIO:63

REX(MM)	TEXT(RAD)	SR(1/SN)
6.775	0.00000	11.71468
9.126	0.00000	4.79469
11.476	0.00000	2.41102
13.826	0.00000	1.37868
16.176	0.00000	0.86085
18.526	0.00000	0.57304
20.876	0.00000	0.40048
23.227	0.00000	0.29080
25.577	0.00000	0.21778
27.927	0.00000	0.16729
30.277	0.00000	0.13128
32.627	0.00000	0.10491
34.977	0.00000	0.08515
37.328	0.00000	0.07006
39.678	0.00000	0.05833
42.028	0.00000	0.04908
44.378	0.00000	0.04169
46.728	0.00000	0.03571
49.078	0.00000	0.03082
51.428	0.00000	0.02679
53.779	0.00000	0.02343

REX(MM)	TEXT(RAD)	SR(1/SN)
6.775	0.53716	10.21250
9.126	0.53716	4.17986
11.476	0.53716	2.10185
13.826	0.53716	1.20189
16.176	0.53716	0.75046
18.526	0.53716	0.49956
20.876	0.53716	0.34913
23.227	0.53716	0.25351
25.577	0.53716	0.18985
27.927	0.53716	0.14584
30.277	0.53716	0.11445
32.627	0.53716	0.09146
34.977	0.53716	0.07423
37.328	0.53716	0.06108
39.678	0.53716	0.05085
42.028	0.53716	0.04279
44.378	0.53716	0.03635
46.728	0.53716	0.03113
49.078	0.53716	0.02687
51.428	0.53716	0.02335
53.779	0.53716	0.02042

REX(MM)	TEXT(RAD)	SR(1/SN)
6.775	0.17905	11.54312
9.126	0.17905	4.72447
11.476	0.17905	2.37571
13.826	0.17905	1.35849
16.176	0.17905	0.84824
18.526	0.17905	0.56465
20.876	0.17905	0.39462
23.227	0.17905	0.28654
25.577	0.17905	0.21459
27.927	0.17905	0.16484
30.277	0.17905	0.12936
32.627	0.17905	0.10337
34.977	0.17905	0.08390
37.328	0.17905	0.06903
39.678	0.17905	0.05748
42.028	0.17905	0.04837
44.378	0.17905	0.04108
46.728	0.17905	0.03519
49.078	0.17905	0.03037
51.428	0.17905	0.02640
53.779	0.17905	0.02308

REX(MM)	TEXT(RAD)	SR(1/SN)
6.775	0.71622	9.11098
9.126	0.71622	3.72902
11.476	0.71622	1.87515
13.826	0.71622	1.07226
16.176	0.71622	0.66952
18.526	0.71622	0.44569
20.876	0.71622	0.31147
23.227	0.71622	0.22617
25.577	0.71622	0.16938
27.927	0.71622	0.13011
30.277	0.71622	0.10210
32.627	0.71622	0.08159
34.977	0.71622	0.06623
37.328	0.71622	0.05449
39.678	0.71622	0.04537
42.028	0.71622	0.03817
44.378	0.71622	0.03243
46.728	0.71622	0.02777
49.078	0.71622	0.02397
51.428	0.71622	0.02083
53.779	0.71622	0.01822

REX(MM)	TEXT(RAD)	SR(1/SM)
0.775	0.89527	7.78615
9.126	0.89527	3.18078
11.476	0.89527	1.60248
13.826	0.89527	0.91634
16.176	0.89527	0.57216
18.526	0.89527	0.38587
20.876	0.89527	0.26618
23.227	0.89527	0.19328
25.577	0.89527	0.14475
27.927	0.89527	0.11119
30.277	0.89527	0.08726
32.627	0.89527	0.06973
34.977	0.89527	0.05660
37.328	0.89527	0.04656
39.678	0.89527	0.03877
42.028	0.89527	0.03262
44.378	0.89527	0.02771
46.728	0.89527	0.02374
49.078	0.89527	0.02049
51.428	0.89527	0.01780
53.779	0.89527	0.01557

REX(MM)	TEXT(RAD)	SR(1/S
6.775	1.07433	6.3228
9.126	1.07433	2.5878
11.476	1.07433	1.3013
13.826	1.07433	0.7441
16.176	1.07433	0.4646
18.526	1.07433	0.3092
20.876	1.07433	0.2151
23.227	1.07433	0.1569
25.577	1.07433	0.1175
27.927	1.07433	0.0902
30.277	1.07433	0.0708
32.627	1.07433	0.0566
34.977	1.07433	0.0459
37.328	1.07433	0.0375
39.678	1.07433	0.0314
42.028	1.07433	0.0264
44.378	1.07433	0.0225
46.728	1.07433	0.0192
49.078	1.07433	0.0166
51.428	1.07433	0.0144
53.779	1.07433	0.0126

APPENDIX C

MICROSTRUCTURES OF EXTRUDED PRODUCTS

In Figs.(C-1),(C-2), some photomicrographs of extruded aluminum products, are given. These show the variation of structure with the initial billet temperature and length of the product.

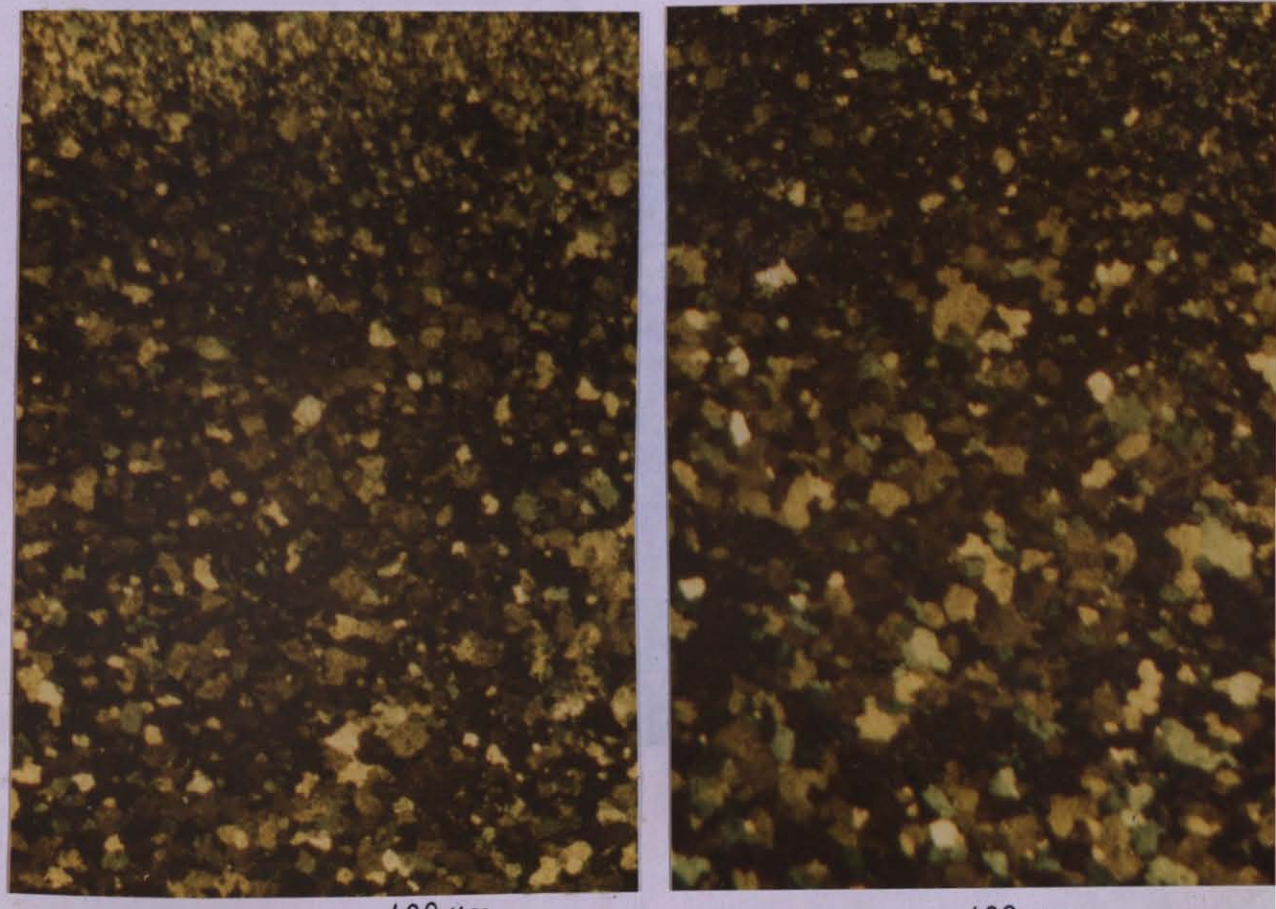

a) R=163, T_o=400°C L = 150 cm b) R=163, T_o=400°C L=300 cm

FIGURE C-1. Variation of surface layer with the length of the product,L.

a) $R = 160$, $T_o = 350^{\circ}C$

b) $R = 160$, $T_o = 400^{\circ}C$

FIGURE C-2. Variation of structure with the initial billet temperature.